國立台灣大學醫學院暨工學院醫學工程研究所

博士論文

Graduate Institute of Biomedical Engineering
College of Medicine and College of Engineering
National Taiwan University
Doctoral Dissertation

膠質母細胞瘤之個人化治療: 以影像生物標記預測腫瘤進展模式與發展對應之腫瘤內藥物傳輸系統

Personalized Glioblastoma Treatment: Seeking Imaging Biomarkers to Predict Tumor Progression Patterns and Developing Targeted Intratumoral Drug Delivery System

梁祥光
Hsiang-Kuang Liang

指導教授：曾文毅 博士、陳中明 博士、林峯輝 博士
Advisors: Wen-Yih Tseng, M.D., Ph.D., Chung-Ming Chen Ph.D., and Feng-Huei Lin Ph.D.

中華民國 106 年 11 月
November 2017

doi:10.6342/NTU201704398

國立臺灣大學博士學位論文
口試委員會審定書

膠質母細胞瘤之個人化治療:以影像生物標記預測腫瘤進展模式與發展對應之腫瘤內藥物傳輸系統

Personalized Glioblastoma Treatment: Seeking Imaging Biomarkers to Predict Tumor Progression Patterns and Developing Targeted Intratumoral Drug Delivery System

本論文係梁祥光君（學號 D02548011）在國立臺灣大學醫學工程學研究所完成之博士學位論文，於民國 106 年 11 月 21 日承下列考試委員審查通過及口試及格，特此證明

口試委員：陳中明　曾文毅

林頌然（指導教授）　鄧厚鑫

林義欽

所長：黃義侑

doi:10.6342/NTU201704398

誌謝

一件事的完成，並非只靠自己一個人，背後有許多人與團隊的幫助。能一路走到這裡，要感謝許多人。

在醫工與臨床研究方面：

感謝曾文毅老師的教導，在研究、教學、人生、信仰，給我許多啟發與鼓勵。感謝陳中明老師的指導，支持我應用不同醫工領域的技術，設計實驗解決臨床問題。感謝林峯輝老師、賴學仕碩士和實驗室團隊，共同合作進行跨領域整合實驗。

感謝台大放射腫瘤科郭頌鑫主任、魏名峰博士、陸思慧物理師與陳亮欣物理師、台大神經外科蔡瑞章主任、曾漢民醫師與賴達明醫師、台大神經部謝松蒼醫師、台大病理部黃佩欣醫師與溫文芬小姐、婦產部周佳宏博士、台大影醫部蘇茂源博士、輔大公衛系游山林教授、台大化工所許朝雄博士、張倖瑋研究助理、台大醫工所林頌然教授、中原醫工系陳民樺教授的參與、建議、討論。感謝台大醫院放射腫瘤科、神經外科、神經部、影像醫學部、病理部、台大醫院神經腫瘤、癌防中心、醫工所辦公室、台北醫學大學放射腫瘤科各單位同仁團隊的協助。感謝一起分享意見，幫助研究的每一個人。特別感謝所有的病人與家屬，每一份資料都是生命歷程的寶貴紀錄。

在「台大輻質中心跨國領航合作計畫」方面：

感謝台大癌症醫院鄭安理院長、楊志新主任支持台大輻質中心跨國合作計畫。感謝台灣大學當時校長楊泮池教授、日本筑波大學永田恭介校長、王碧昭教授、大庭良介教授、筑波大學醫院松村明院長、筑波質子中心櫻井英幸部長、坪井康次教授、武榮二教授、水本斉志醫師，在雙邊各位師長與同仁協助下，開啟台大輻質中心與筑波大學質子中心合作研究與交流訓練計畫。

感謝北海道大學醫院、MD Anderson Cancer Center、St. Jude Children's Research Hospital、Proton Therapy Center in San Diego 的 faculty 接待台大輻質中心跨國合作計

doi:10.6342/NTU201704398

畫參訪行程。感謝 MD Anderson Cancer Center Ueno Naoto 教授和 Japan Team Oncology Program Committee 讓我加入腫瘤團隊合作學院 faculty 的行列。

感謝全民健康基金會與董事長許金川教授關注質子治療對台灣癌症發展的重要性，支持獎助台灣質子治療與國際連結合作計畫，並給予我許多進修發展的寶貴建議與鼓勵。感謝永齡健康基金會與創辦人郭台銘先生捐贈台大輻質中心，以及一同執行計畫的團隊。感謝台大癌醫籌備處團隊，提供台大輻質中心跨國合作計畫的幫助。

在人生歷程方面：

感謝我的父母，雖因癌症過世多年，但他們的生命就像「一粒麥子落在地裡，結出許多子粒來」。感謝我的岳父，他以前在世看見告訴我的，如今我漸漸看見。感謝我的岳母、叔叔、嬸嬸時常為我們家禱告，愛我們的家，全力支持我所做的事。感謝許多親人、朋友、兄弟姊妹、同學、同事，時常關心、鼓勵、幫助。感謝士林、以琳、Tsukuba International Christian Assembly 以及許多教會弟兄姊妹關心代禱。感謝在日本許多來自台灣與世界各國的朋友幫助我們在筑波進修的生活。

從物理系、醫學系到醫工所，從神經部、放射腫瘤科到台大輻質中心，一路走來經歷挑戰、挫折、停頓、計畫未過、論文退稿，幾度感到灰心疑惑。每當想起這些病人，其中有我照顧過的病人、同事、同學、親人、朋友，「希望幫助治好更多人」的念頭讓我又繼續前進。

持守信念，人生總會遇到理念相同的人，相互支持鼓勵。

特別感謝太太的支持，孩子的陪伴，還有

天父、耶穌、聖靈一路保守帶領。

這一刻，想起許多令我感謝與懷念的人。我只能忘記背後，努力面前，繼續向著標竿直跑…

doi:10.6342/NTU201704398

中文摘要

膠質母細胞瘤為成人最常見原發型腦瘤。同步放化療後最常見的進展型態為局部或照野內復發，約佔 72%–96.8%，而遠端轉移或照野外復發約佔 2%–28%。病人開刀前若有腫瘤周邊水腫大範圍延伸以及腫瘤位於腦室和胼胝體交界處，存活較差並有多樣化進展型態。我們以影像生物標記，分類膠質母細胞瘤病人的腫瘤進展型態，包括侷限型、中間型和擴散型，與相對應不同的存活狀況。再根據不同分類，提出相對應的膠質母細胞瘤放射治療目標劃定與劑量給予，決定個人化的治療策略。侷限型膠質母細胞瘤僅有小於 10%的人腫瘤會延伸大於原腫瘤界線兩公分，然而擴散型病人，超過 70%會有腫瘤移動超過原腫瘤界線兩公分的情況。和侷限型的病人相比，擴散型的病人存活狀況較差。我們的臨床研究顯示需要根據膠質母細胞瘤影像生物標記制定個人化的治療策略。

無論侷限型或擴散型，原腫瘤處是膠質母細胞瘤復發最常見的位置。提高腫瘤局部控制的最好策略之一，就是腫瘤內藥物注射再加上局部放射治療。我們比較各種腫瘤內藥物傳輸方式，包括藥片、熱塑型水膠和對流加壓注射，比較藥物釋放安全性與輻射增強效果，設計一個基礎研究探討腫瘤內藥物傳輸方式，以便臨床應用。

為達到未解決的臨床需求，我們合成一個新的藥物結合水狀凝膠與卡鉑進行腫瘤內藥物注射。經過全面性的生物材料、細胞與動物實驗，我們成功證實水狀凝膠與卡鉑是一個安全、有效、方便的藥物組合。腫瘤內卡鉑凝膠注射保有放射化學治療的協同效果，而且沒有嚴重的治療副作用。單次腫瘤內水狀凝膠與卡鉑注射的藥物持續釋放，簡化給藥過程與接續的放射治療，有助應用在臨床腦瘤治療。

關鍵字: 膠質母細胞瘤、影像生物標記、疾病分類、個人化治療、卡鉑凝膠、腫瘤內藥物注射、同步放射化學治療

doi:10.6342/NTU201704398

ABSTRACT

Glioblastoma is the most prevalent primary brain tumor of adults. The most common progression patterns after concurrent chemoradiotherapy are local and in-field (72%–96.8%), and the rates of distant and out-field recurrence range from 2% to 28%. The extensive preoperative edema (EPE) (edema extent ≥ 2 cm from the tumor edge) and tumor located at synchronous subventricular zone and corpus callosum (sSVZCC) are associated with poor survival and diverse progression patterns of glioblastoma. We combined the imaging biomarkers, EPE and sSVZCC invasion, to classify glioblastomas progression patterns, including confined, intermediate, and extensive types, with different survivals. According to the classification, we proposed the corresponding RT target volume delineations and dose prescriptions to personalize treatment strategies for glioblastomas.

Less than 10% of patients with EPE- (confined type) have tumor progression extending beyond the 2-cm margin from the preoperative tumor edge, while more than 70% glioblastomas with EPE+/SVZCC+ (extensive type) have tumor migration beyond the 2-cm margin from the preoperative tumor edge along the preoperative edema areas. Compared with patients with confines type glioblastoma, those with extensive type have poorer survival. Our clinical study demonstrated the need for developing individualized irradiation strategies for glioblastomas according to the imaging biomarkers of EPE and sSVZCC invasion.

The tumor bed is the most common recurrence area of glioblastomas either confined or extensive types. One of the strategies to increase the local tumor control is intratumoral drug delivery combining with local radiotherapy (RT). We compared the drug release and safety features of intratumoral delivery modalities (wafer, thermogelling hydrogel, and convection-

doi:10.6342/NTU201704398

enhanced delivery) and the radiosensitizing effects among anti-cancer drugs (carmustine, carboplatin, and cisplatin) to propose a basic investigation on the intratumoral drug delivery for further clinical application.

To satisfy the unmet clinical need for glioma treatment, we compounded a novel drug combination of oxidated hyaluronic acid/adipic acid dihydrazide hydrogel and carboplatin for intratumoral injection. Through the comprehensive biomaterial, cell, and animal experiment design, we significantly demonstrated that hydrogel carboplatin is a safe, effective, and convenient drug combination. Intratumoral hydrogel carboplatin injection simplified the method and frequency of intratumoral hydrogel carboplatin delivery and remained the RT synergistic effect without causing severe toxicity, which makes intraoperative single drug injection with subsequent RT a feasible and potential clinical treatment for glioblastomas.

Keywords: glioblastoma, imaging biomarkers, disease classification, personalized treatment strategy, hydrogel carboplatin, intratumoral drug injection, concurrent chemotherapy

doi:10.6342/NTU201704398

TABLE OF CONTENTS

doi:10.6342/NTU201704398

doi:10.6342/NTU201704398

doi:10.6342/NTU201704398

doi:10.6342/NTU201704398

doi:10.6342/NTU201704398

doi:10.6342/NTU201704398

doi:10.6342/NTU201704398

CHAPTER 1 INTRODUCTION

1.1 Glioblastomas: Epidemiology, Pathology, and Treatment Outcomes

Gliomas are the most prevalent primary intracranial tumor of adults, representing 81% of brain tumors and the most common malignant glioma histology is glioblastoma, which accounts 45% of all gliomas, follow by anaplastic astrocytoma [1]. There are annually 150 to 200 glioblastoma cases which accounts for about 37% to 47% of adult primary brain tumor in Taiwan, and the male-to-female ratio of incidence is around 1.3 to 1.5 [2-4]. The histological features of glioblastoma include increased cellularity, mitotic activity, microvascular proliferation, nuclear atypia, and necrosis [5], which are correlated to the typical image findings of central areas necrosis with extensive peritumoral edema [6].

Clinically, common prognostic factors for glioblastoma patients include age, Karnofsky performance status (KPS), neurologic status, and tumor resection extent [7-9]. The molecular biomarker of isocitrate dehydrogenase 1 (IDH1) mutation significantly predict patient overall survival (OS) [10, 11]. Before the invention of temozolomide, an alkylating agent for treating malignant glioma, surgical resection followed by radiotherapy (RT) resulted in a better OS than resection without RT [12]. Nowadays, surgical resection followed by concurrent chemoradiotherapy (CCRT) with oral temozolomide became the standard treatment for glioblastoma. The methylation status of O^6-methylguanin-deoxyribonucleic acid (DNA) methyltransferase (MGMT) promotor substantially identifies patients most likely to benefit from CCRT with temozolomide [10]. The median OS and 2-year survival rates for patients receiving definitive or adjuvant CCRT with temozolomide are 13.4–16.0 months and 26.5%–31%, respectively [13-15].

doi:10.6342/NTU201704398

1.2 The Clinical Unmet Needs for Glioblastomas: Individualized Treatment Strategies According to the Progression Patterns

The most common progression patterns after CCRT with temozolomide are local and in-field (72%–96.8%), and the rates of distant and out-field recurrence range from 2% to 28% [16-18]. However, the clinical prognostic factors and available molecular biomarkers do not correlate with the glioblastoma progression patterns, in-field or out-field, after CCRT. Clinically, there is no effective factor available to predict whether the tumor progresses confined to the tumor bed or spreads out of tumor bed. To develop individualized treatment strategy for glioblastomas of different progression patterns, effective factors are required for disease classification [19].

Currently, RT guidelines adopted by the European Organisation for Research and Treatment of Cancer (EORTC) and the Radiation Therapy Oncology Group (RTOG) for target delineation and dose prescription of the peritumoral edematous areas of glioblastoma are diverse [20]. The necessity of irradiating peritumoral edema of glioblastomas remains controversial. The EORTC uses a 2-cm volumetric expansion of the gross tumor volume (GTV) to generate the clinical target volume (CTV) in a single phase of 60 Gy in 30 fractions, which is based on published data stating that > 80% of recurrences occur within a 2-cm margin of contrast-enhanced lesions by computed tomography (CT) or magnetic resonance imaging (MRI) scans [20]. The RTOG defines CTV1 as the surgical resection cavity plus any residual enhancing tumor plus surrounding edema within a 2–2.5-cm margin, which should receive 46 Gy in 23 fractions, followed by a cone-down boost to the tumor bed with a 2-cm margin, while CTV2 should receive an additional 14 Gy in seven fractions [20], considering that pre- or postmortem findings have demonstrated high rates of glioblastoma cells at

doi:10.6342/NTU201704398

peritumoral edema areas, as observed in CT and MRI scans [21].

Some studies reported that glioblastomas with subventricular zone (SVZ) or corpus callosum (CC) invasion are associated with adverse prognoses and diverse progression patterns [22-24]. Patients with glioblastoma involving the SVZ are highly associated with a significant decline in progression-free survival (PFS) and OS [24-26]. Some published data demonstrated that glioblastoma with SVZ invasion is associated with local recurrence as well as spreading to the ventricles, distant areas, and multifocal progression [22, 24, 27, 28]. Similarly, glioblastoma with preoperative contrast-enhanced tumors or edema involving the CC [9, 29] and butterfly glioblastoma, a tumor involving the bilateral hemispheres through the CC, [30, 31] are poor prognostic factors for OS. In addition to SVZ and CC invasion, extensive peritumoral edema observed on T2-weighted or fluid-attenuated inversion recovery (FLAIR) MRI images is associated with a poor prognosis for glioblastoma patients [32].

The tumor bed is the most common recurrence area of glioblastomas and one of the treatment strategies to increase the local tumor control is intratumoral drug delivery which has the advantage of reducing the systemic toxicity and circumventing the blood-brain barrier [33]. Three modalities, including wafer, convection-enhanced delivery (CED), and hydrogel, were proposed for intratumoral anti-cancer drug delivery [33-35]. Nowadays, only carmustine wafer was utilized clinically for glioblastoma as intratumoral drug delivery [34, 35].

The individualized treatment strategies for glioblastoma patients according to their progression patterns remained undetermined. Figure 1 illustrates our study concept to satisfy the clinical unmet needs for glioblastomas, we proposed an extensive study, including

doi:10.6342/NTU201704398

clinical and basic investigations, to explore imaging biomarkers for glioblastoma classification and intratumoral drug injection for glioblastoma treatment, respectively.

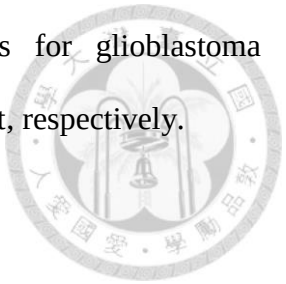

1.3 Clinical Investigation of Imaging Biomarkers: Hypothesis and Purpose

The neurogenesis of adult mammalian brain occurs in the SVZ on the walls of the lateral ventricles and the subgranular layer of the dentate gyrus in the hippocampus [36-38]. In humans, the anterior, occipital, and temporal horns of lateral ventricles comprise different astrocytes and ependymal, proliferating cells, and migratory patterns [36]. Cerebral commissures, including the CC and the anterior commissure, contribute interhemispheric connections. The anterior (the genu) and posterior (the splenium) sections of the CC connect the bilateral frontal and occipital lobes through the radiating fibers, respectively. The ventral surface of the CC forms the roof of the lateral ventricles close to the SVZ [39]. The anterior commissure comprises a bundle of axons, which crosses the midline in the lamina terminalis and traverses the corpora striata, and supplies communication between the temporal lobes [39]. The peritumoral edema of glioblastoma correlates with cancer cell infiltration [21] or effusion resulting from blood-brain barrier damage [40].

The SVZ hosts potential neural progenitor cells, the CC provides the interhemispheric connections, and the preoperative edema (PE) correlates with cancer cell infiltration. Using the imaging biomarkers including the anatomical factors (SVZ and CC) [23] and pathophysiological factors (PE), we investigated the outcome of glioblastoma after CCRT and classified patients according to the survival and progression patterns. The classification

doi:10.6342/NTU201704398

categorized glioblastoma with in-field (confined near the tumor bed) or out-field (spreading beyond the tumor bed), which requires individualized treatment strategy.

From the anatomical perspective, we hypothesized that glioblastomas with synchronous SVZ and CC (sSVZCC) invasion have distinct progression patterns associated with the interhemispheric and lateral ventricular involvement. From the pathophysiological perspective, we hypothesized that glioblastomas with extensive PE (EPE) have high tumor migration ability. For glioblastoma patients, the interactions between the anatomical factor sSVZCC and the pathophysiological factor EPE and the associated clinical impacts, including tumor migration ability and directions, remain undetermined (Figure 2). We analyzed the associations between these imaging factors and survival and tumor progression patterns after CCRT to classify glioblastomas for further proposing individualized treatment strategies.

1.4 Basic Investigation of Intratumoral Drug Injection: Hypothesis and Purpose

Clinically, carmustine (an alkylating agent) is delivered by local wafer implantation during surgery after tumor resection to improve the survival [34, 35]. Carmustine is released from wafers over a period of approximately 5 days and wafers degrade completely over a period of 6 to 8 weeks when in continuous contact with interstitial fluid [41]. However, the adverse effects of carmustine wafer, such as healing abnormalities, cerebral edema, cerebrospinal fluid leaks, and intracranial infection were reported [34]. Big resection cavity size required for adequate drug dosage or implant dislodgement result in the technique

doi:10.6342/NTU201704398

difficulty [42]. Besides, the synergistic effect of combining carmustine with RT for malignant gliomas was limited [49].

Carboplatin is a platinum-based antineoplastic agent, which is widely combined with radiotherapy for clinical cancer treatment [43-45]. Carboplatin binds to DNA to form intrastrand and interstrand cross links with the purine bases [46] and thus enhances the formation of cluster damage to DNA by ionizing radiation [47]. Several animal studies demonstrated the synergistic effect of combined carboplatin and radiation for glioma treatment [48-50]. However, carboplatin delivered by intratumoral infusion via the CED is limited in clinical practice due to the complications and delivery difficulty [49, 51]. The complications caused by CED include increased brain edema, infection, bleeding, and seizures [52]. The difficulty in catheter placement surgery depends on the brain lesion locations [52]. Moreover, neurotoxicity can be induced by the infusate backflow in the catheter, which can not be completely prevented by any insertion method [53].

The oxidized hyaluronic acid/adipic acid dihydrazide (oxi-HA/ADH) hydrogel is a biocompatible and thermogelling material [54], which can transform from liquid form into a gel-like matrix within 1–8 min, depending on the operational temperature [54]. Oxi-HA/ADH hydrogel is stable at body temperature. It maintains its gel-like state for up to 5 weeks after in vivo injection and is degraded gradually by hyaluronidase [54]. To meet requirements, including slow and steady release and radiosensitizing effect and to avoid the difficulties of wafer implantation and CED catheter placement [41, 48-50, 52], some studies investigated the combination of hydrogel-loaded anticancer agents for glioma treatments, including temozolomide, gemcitabine, cisplatin, and methotrexate etc. [42].

doi:10.6342/NTU201704398

The ability of oxi-HA/ADH hydrogel to carry hydrophilic drug by crosslink achieves slow and steady drug release. Carboplatin has more intensity to produce DNA double-strand breakage than cisplatin as regard to the synergistic effect with ionized radiation, [47]. Combining these features, thermogelling oxi-HA/ADH hydrogel is potential to load carboplatin for single intratumoral injection to simplify the delivery method and frequency without compromising the synergetic effect of RT [55-58].

In Figure 3 [59], we compared the drug release and safety features of intratumoral delivery modalities (wafer, thermogelling hydrogel, and CED) [33-35] and the radiosensitizing effects among anti-cancer drugs (carmustine, carboplatin, and cisplatin) [47, 60]. In the current study, we proposed a novel combination of carboplatin loaded by thermogelling oxi-HA/ADH hydrogel and RT to satisfy the unmet clinical needs for treating malignant gliomas. The effectiveness, convenience, and safety of intratumoral delivery of oxi-HA/ADH hydrogel carboplatin (briefly hydrogel carboplatin) combined with RT for treating gliomas remains undetermined. From the biomedical engineering perspective, we hypothesized the sustained release of hydrogel carboplatin simplifies the drug delivery method and frequency and remains the synergistic effect with RT and without severe toxicity. Through the comprehensive biomaterial, cell, and animal experiment design, we intended to demonstrate that the synergistic effect with RT by using single injection of hydrogel carboplatin is comparable to multiple injections of aqueous carboplatin. In addition, we used different regimens, including drug forms and dosages, to find the optimal CCRT parameters to improve the local tumor control and survival for mice glioma treatment, which makes intraoperative single drug injection with subsequent RT a feasible and potential clinical treatment for glioblastomas.

doi:10.6342/NTU201704398

CHAPTER 2 MATERIALS AND METHODS

2.1 Clinical Study of Imaging Biomarkers

2.1.1 Patient eligibility

Patients from a single institute (National Taiwan University Hospital), who were pathologically confirmed as having glioblastoma between August 2004 and December 2015, were retrospectively evaluated after receiving approval from the institute's institutional review board (201405076RINC). Patients who received complete CCRT with temozolomide were enrolled and were excluded if they were younger than 18 years, had active concomitant malignancies, received an RT dosage of < 54 Gy, or did not receive follow-up MRI or CT scans after CCRT.

2.1.2 Treatment modalities

The extent of tumor excision was classified as gross total and subtotal resection. Biopsy was employed for unresectable lesions.

RT techniques [23], including three-dimensional conformal RT, intensity-modulated radiation therapy, volumetric-modulated arc therapy, and tomotherapy, were employed using 6-MV linear accelerators. GTV1 was defined as gadolinium-enhanced lesions on T1-weighted images and hyperintense lesions on FLAIR or T2-weighted images. GTV2 was defined as gadolinium-enhanced lesions on T1-weighted images. CTV1 and CTV2 were defined, respectively, as the GTV1 and GTV2 plus a 1.5–2-cm margin for potential microscopic disease with a margin reduced to 0.5 cm around natural boundaries or the optic nerve/chiasm. The planning target volume (PTV)1 and PTV2 were CTV1 and CTV2 plus a 0.3–0.5-cm margin, respectively. An RT dosage of 46 Gy—administered at a daily dose of 2

doi:10.6342/NTU201704398

Gy once per day for 5 days per week—was prescribed for PTV1, and an additional 14 Gy was prescribed for PTV2. Uninvaded SVZ was not irradiated in this study.

Concurrent chemotherapy with temozolomide was administered at a daily dose of 75 mg/m^2 for 7 days per week, from the first to the last day of RT. After a four-week break, the patients received up to six cycles of adjuvant temozolomide for 5 days over a 28-day period. The dose was 150 mg/m^2 for the first adjuvant cycle, and this was increased to 200 mg/m^2 at the beginning of the second cycle [15].

2.1.3 Anatomical features of preoperative imaging

Neuroimaging (MRI or CT) findings were interpreted by neuroradiologists. Preoperative imaging findings, including tumor size, edema extent, and anatomical invasion into the SVZ and CC, were evaluated. PE was defined as a hyperintense area observed through T2 or FLAIR MRI or a hypointense area observed through CT. We used the MRI hyperintense signal on T2W or FLAIR sequence with different sections, including axial, coronal, and sagittal sections, to measure the edema distance along the normal line from tumor margin to the distal edema edge. The method of evaluating the preoperative edema extent is illustrated in Figure 4. First, we selected the image section that presented the maximum diameter of the preoperative tumor (Figure 4A). Then, we created a 2-cm expansion of the tumor edge along the SVZ (the lateral wall of lateral ventricles) or CC if these structures are invaded (Figure 4B); otherwise, we drew tangential lines to the tumor edge and then used their normal lines to expand a 2-cm margin of the tumor. The 2-cm expansion margin of the tumor was used as the reference boundary to evaluate the PE extent. The 2-cm expansion margin of the preoperative tumor was applied on the similar image

doi:10.6342/NTU201704398

sections after concurrent CRT to evaluate the PD extent.

EPE was defined as PE extending ≥ 2 cm from the tumor margin (Figure 5, A1). sSVZCC invasion was defined by the presence of contrast-enhanced lesions synchronously involving the lateral walls of the lateral ventricles and cerebral commissures (the CC or anterior commissure) [23] as illustrated in Figure 5, A2. The neural fiber tracts (NFTs) included the CC, forceps frontalis, and forceps occipitalis, defined by anatomical structures [39] (Figure 5, A2). For tumors with sSVZCC invasion, the EPE along the CC (CCEPE) and along the SVZ (SVZEPE) were defined as edema extending ≥ 2 cm from the tumor margin along the CC and the SVZ, respectively (Figure 5, A2). Tumor size was defined by the maximum diameter determined through preoperative T1-weighted gadolinium-enhanced MRI or contrast-enhanced CT scans [61].

2.1.4 Tumor progression patterns after CCRT

Neuroimaging after CCRT was performed primarily through MRI at intervals of 3–6 months. Tumor progression was assessed according to the imaging definition of Response Assessment in Neuro-Oncology criteria and involved either of the following: (1) ≥ 25% enlargement of contrast-enhanced lesions compared with the smallest tumor measured either at the baseline (if no decrease) or at best response, or (2) appearance of any new contrast-enhanced lesions [62, 63]. When early progressive disease is suspected on the images within 12 weeks after completion of concurrent CRT, we used the following criteria to differentiate it from the pseudoprogression: the presentation of new enhancement beyond the radiation field or the high-dose region [62, 63]. Reoperation for pathological confirmation was

doi:10.6342/NTU201704398

accepted according to neurosurgeons' clinical judgement for differentiating tumor progression from pseudoprogression and radiation necrosis [62, 63].

Extensive progressive disease (EPD) was defined as the progression of tumors continuously extending or discretely spreading ≥ 2 cm from the preoperative tumor margin along the PE areas (Figure 5, A3) [64]. For tumors with sSVZCC invasion, EPD in the SVZ (SVZEPD) and in the CC (CCEPD) were defined as tumors continuously extending or discretely spreading with PE areas along the SVZ and the CC, respectively, for ≥ 2 cm from the preoperative tumor margin (Figure 5, A3). We adopted the two imaging factors of EPE and sSVZCC invasion to categorize patients into four groups (Figure 5; B1,2 and C1,2) to analyze the survival, EPD rate, and tumor progression patterns (Figure 5, B3 and C3). The tumor progression areas were categorized as local (tumors involving the original tumor bed), regional (tumors involving the preoperative edematous areas and located beyond the original tumor bed), and distant (tumors located beyond the original tumor bed and preoperative edematous areas) [23].

2.1.5 Statistical analysis

Data analysis and statistical tests were performed using SPSS (version 19; SPSS, Chicago, IL, USA). OS was calculated on the basis of the date of first histological diagnosis to the date of death. PFS was calculated on the basis of the date of first histological diagnosis to the date of disease progression, including death or tumor progression proven through imaging Patients lost to follow-up or those who were alive but were without progression at the time of analysis were censored from the analysis. Survival was calculated using the Kaplan-Meier product-limit method. Differences in survival were compared between the

doi:10.6342/NTU201704398

groups by using the log-rank test. The variables of the anatomical features and other adverse prognostic factors, including age, KPS, extent of tumor resection, and tumor size, were used for the univariate and Cox regression analyses [7-9, 61, 65]. Patient age was stratified as < 50 versus ≥ 50 years, KPS as ≤ 70 versus ≥ 80, and tumor size as < 5 versus ≥ 5 cm. The extent of tumor excision was classified according to the findings of postoperative neuroimaging or neurosurgeon records. The hazard ratios (HRs) and 95% confidence intervals (CIs) were calculated for the survival data. Fisher's exact test was used to examine the significance of the association between EPE and sSVZCC invasion and tumor progression patterns and areas. All tests were two-sided and results with $p < 0.05$ were considered statistically significant.

2.2 Basic Study of Intratumoral Hydrogel Carboplatin Injection

The workflow of our comprehensive study design, including biomaterial, in vitro, and in vivo investigations, is illustrated in Figure 6 [59].

2.2.1 Biomaterial investigation

The materials and reagents used for the preparation of hydrogel carboplatin were: hyaluronic acid (HA, average molecular weight 1.5–1.8 × 10^6 Da), adipic acid dihydrazide (ADH), sodium bicarbonate, and sodium chloride (Sigma-Aldrich, Missouri, USA), ethylene glycol and sodium periodate ($NaIO_4$) (RDH Chemical Company, California, USA), dialysis bag MWCO 6000–8000 (Spectrum Laboratories Incorporated, California, USA), and

doi:10.6342/NTU201704398

PARAPLATIN® (carboplatin aqueous solution, 10 mg/mL) (Bristol Myers Squibb Company, New York, USA).

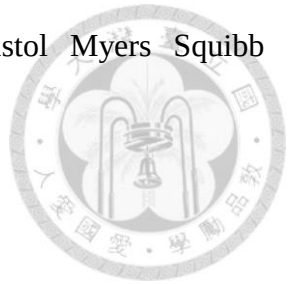

2.2.1.1 Preparation of oxi-HA/ADH hydrogel and hydrogel carboplatin

The procedures of oxi-HA/ADH hydrogel and hydrogel carboplatin preparation were illustrated in Figure 7A and 7B [59]. One gram of HA powder was dissolved in 100 mL of double-distilled water to form a weight percentage 1% (w/v) aqueous solution of hyaluronic acid, and then 15 mL of sodium periodate solution ($NaIO_4$, 2.67%) were added gradually with stirring. The molar ratio of $NaIO_4$ to HA was 1:1 to achieve oxidation degrees [54]. After 24 h at room temperature, the oxidation reaction was ended by adding ethylene glycol for 30 minutes. The oxi-HA solution was poured into a dialysis bag MWCO 6000-8000 with water changed twice daily for 3 days. The final products were dried by a freeze dryer (FDU-1100, EYELA, Tokyo, Japan) for 3 days to yield a white fluffy product, oxi-HA [54]. The oxi-HA was dissolved in a phosphate-buffered saline (PBS, pH 7.4) to a concentration of 6% (w/v) at a 4 °C overnight. At the same temperature, 0.24 mg of ADH dissolved in 3 mL of aqueous carboplatin (10 mg/mL) were homogeneously mixed to form ADH carboplatin solution. Afterwards, 12 mL of oxi-HA was added into the mold, and then 3 mL of ADH carboplatin solution was slowly poured and mixed to form hydrogel carboplatin [66], with the carboplatin concentration of 2 mg/mL.

2.2.1.2 Characterization of oxi-HA/ADH hydrogel and hydrogel carboplatin by Fourier transformation infrared (FTIR) analysis

doi:10.6342/NTU201704398

An FTIR spectrometer, FTIR-4200 (JASCO Incorporated, *Maryland*, USA), with ATR PRO450-S was used to distinguish the functional groups of oxi-HA, ADH, oxi-HA/ADH, and hydrogel carboplatin. Freeze-dried samples were ground into power, placed in well plates, and then pressed down gently by the pressure tip. The FTIR spectra were recorded by 16 scans between 2500 and 500 cm^{-1} with a resolution of 8 cm^{-1} [54].

2.2.1.3 Gelling time and temperature of oxi-HA/ADH hydrogel by rheometer

A rheometer DHR-3 (TA instruments, USA) with cone and plate geometry were used to estimate the rheological properties of oxi-HA/ADH hydrogel. The elastic modulus G' and the viscous modulus G" were record and analyzed by TRIOS software (TA instruments, USA) [67]. The crossover point (called the gel point) of G' and G" determined the gel formation and the gelling time of substance as the time elapsing from liquid state to gel state [54]. The G' and G'' crossover point of oxi-HA/ADH hydrogel was used to evaluate the gelling time at different temperatures ranging from 4 to 40 °C, which was measured by oscillation time sweep mode at 0.1 Hz, 10 Pa and terminated after 15 min [67].

2.2.1.4 Degradation property of oxi-HA/ADH hydrogel

In PBS under 37 °C, 5% CO_2, 0.3 mL of liquid-state oxi-HA/ADH solution was poured into the cylinder mold and put for 10 min to form a gel-like matrix. Then the cylinder of oxi-HA/ADH hydrogel was moved into a 24-well culture plate and 3 mL PBS was added to each well [54]. At 12, 24, 72 and 120 h, the oxi-HA/ADH hydrogel was taken out respectively. Lyophilization of the hydrogel was performed by using a freeze-drying method to obtain the

doi:10.6342/NTU201704398

dry weight (Wd). The degradation percentage was calculated with the formula (Wd-Wi)/Wi × 100%, where Wi is the initial weight of hydrogel at hour 0 [54].

2.2.1.5 Drug release profile of hydrogel carboplatin by inductively coupled plasma mass spectrometry (ICP-MS)

At 4 °C, 0.24 mL of 6% (w/v) Oxi-HA solution and 0.06 mL of 8% (w/v) ADH carboplatin solution were mixed in the mold to form hydrogel carboplatin. After 10 minutes, the hydrogel carboplatin was extracted from the mold and put into 24 well. After that, 3 mL of PBS (pH=7.4) was poured into each well. The 24 well contained the hydrogel carboplatin and PBS were incubated in the shaking bath (37 °C, 50 rpm). The release medium was removed at scheduled time points (1, 3, 6, 12, 24, 48, 72, 96, and 120 h) for sampling and replaced immediately with fresh PBS to keep the sink condition. The sampled carboplatin content in the release medium was measured by ICP-MS to calculate and draw the cumulative release curve [68].

2.2.2 In vitro investigation

The materials and reagents used were: Firefly D-luciferin potassium salt (Biosynth Incorporated, Naperville, USA), ALTS1C1 (glioma cells, BCRC, Taiwan) with the luciferase gene (National Centre for Cell Sciences, Taipei, Taiwan), 3T3 cells (BioVision, USA), Dulbecco's modified Eagle's medium/high glucose (Sigma-Aldrich), trypsin-EDTA, fetal bovine serum (FBS) and antibiotic-antimycotic solution (Gibco, Waltham, USA), Quick Cell Proliferation Assay Kit and Cytotoxicity Assay Kit (Takara, Japan), water-soluble

doi:10.6342/NTU201704398

tetrazolium-1 (WST-1, Takara) and LIVE/DEAD Viability/Cytotoxicity Kit (Invitrogen, Carlsbad, USA).

2.2.2.1 Cell culture

ALTS1C1 cells and 3T3 cells were preserved in the high glucose medium supplied with 10% FBS and 1% antibiotic–antimycotic.

2.2.2.2 Biocompatibility of oxi-HA/ADH hydrogel

Biocompatibility of oxi-HA/ADH hydrogel was assessed by examining the extraction medium with 3T3 cells according to International Standardization Organization standards [69]. The extraction medium was prepared by incubating the oxi-HA/ADH hydrogel with standard culture medium at a 0.75 cm^2 mL^{-1} extraction ratio for 72 h at 37 °C [54]. Two hundred microliters of the extraction medium were examined on a monolayer of 3T3 cells seeded in 96-well tissue culture plates and fed with standard culture medium at 37 °C under 5% carbon dioxide atmosphere. The study groups included control (standard culture medium), negative control (Al_2O_3 extraction medium), positive control (0.2 g/mL zinc diethyldithiocarbamate contained medium), and experimental group (oxi-HA/ADH hydrogel extraction medium) [54]. After incubation at 37 °C for 72 h, biocompatibility evaluations, including cell viability and cytotoxicity, were quantitatively analyzed.

For cell viability evaluation, the test medium was abandoned and 0.2 mL of WST-1 working solution was moved to each well. After 2 h incubation, the WST-1 working solution

doi:10.6342/NTU201704398

should show color change because the tetrazolium salt split and formed formazan by cellular mitochondrial dehydrogenase. The viability of 3T3 cell was quantitatively analyzed by the ELISA reader (Tecan, Sunrise, Switzerland) readout at 450 nm with the reference wavelength of 650 nm [54].

For cytotoxicity evaluation, 0.05 mL of the incubation medium was moved into 96-well ELISA plates (Tecan, Sunrise, Switzerland) and mixed with 0.05 mL of substrate mix, then was incubated for 30 min in the dark. The tetrazolium salt in substrate mix could react with lactate dehydrogenase (LDH) to give a red formazan product. LDH released in the medium was quantitatively analyzed by ELISA reader readout at 490 nm using extraction medium without incubating 3T3 cells as a culture medium background. The 3T3 cells were lysed by lysis solution (1% Triton® X-100) and the OD 490 value was recorded [54]. The cytotoxicity percentage was calculated with the formula (Medium OD – Blank OD)/ (Total lysis – Blank OD) x 100%, where OD is the optic density [54].

Two fluorescent dyes, calcein-AM (a non-fluorescent molecule, Invitrogen, Carlsbad, USA), and ethidium homodimer (EthD-1, Invitrogen, Carlsbad, USA) were used in the LIVE/DEAD staining kit. Calcein-AM could be hydrolyzed by intracellular esterase into the highly negatively charged green fluorescent calcein to identify live cells. EthD-1 is a high-affinity nucleic acid stain that is weakly fluorescent until bound to DNA, yielding a bright red fluorescence to identify dead cells [54]. 3T3 cells treated with extraction medium were stained with LIVE/DEAD staining kit and photographed by confocal microscope (Olympus, Japan).

doi:10.6342/NTU201704398

2.2.2.3 Half maximal inhibitory concentration (IC_{50}) of carboplatin to ALTS1C1 glioma cells

ALTS1C1 cells were preserved in high glucose medium supplied with 10% FBS and 1% antibiotic–antimycotic. Cells were plated in a 96-well plate with a density of 10^4 cells per well in 0.2 mL of complete medium. After 24 h, 0.02 mL of the concentrated carboplatin solution was poured to each well to accomplish the final concentration ranging from 0.1 to 100 mg/mL. A control group was treated with 0.02 mL of PBS. Cells were incubated for either 1-day or 3-day treatment before the cell assay [55]. The cell viability was evaluated by the WST-1 assay. At the end of each treatment, the medium was replaced with 0.2 mL of fresh medium containing 0.02 mL WST-1 solution and was incubated for 2 h. The absorbance of the solubilized formazan was recorded with an ELISA reader at a wavelength of 450 nm with the measured absorbance normalized to the absorbance of PBS-treated cells [55].

2.2.3 In vivo investigation

This animal experiment was approved by the ethical committee for animal care of National Taiwan University and was performed following the national regulations' guidelines. Mice (C57BL/6) were purchased from BioLASCO Co. (Taipei, Taiwan).

2.2.3.1 Subcutaneous tumor implant model of mice

Subcutaneous glioma implants model was adopted to monitor tumor volume serially according to published studies [70-72]. Six-week-old male C57BL/6 mice were used and ALTS1C1 glioma cells with luciferase reporter gene [73, 74] were injected subcutaneously

doi:10.6342/NTU201704398

in their right thigh [70, 71]. When the tumor diameter grew up to 3 to 4 mm and adequate for intratumoral drug injection, mice were categorized into different treatment groups.

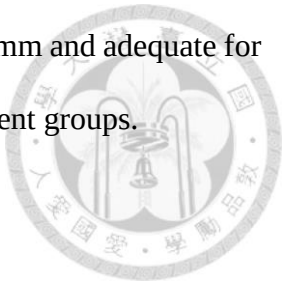

2.2.3.2 Intratumoral dye injection

Blue colorant (20 μL) containing methylene blue (Sigma-Aldrich, Missouri, USA) was mixed with oxi-HA/ADH hydrogel (80 μL) and injected into the subcutaneous tumor via a syringe with a 28-gauge needle. The mice were sacrificed 1 day and 3 days after intratumoral dye injection respectively, followed by tumor excision and gross section to evaluate the distribution of dye loaded by hydrogel [49].

2.2.3.3 Irradiation setting

The mice were anesthetized by intramuscular injection (1 μl/g) of a mixture with Zoletil 50 (Virbac Laboratory, France) and 2% Xylazine (Bayer, Germany) in a 2:1 ratio [75, 76]. The radiation was delivered with 20 Gy (10 Gy daily fraction for 2 fractions, at a dosage rate of 0.5 Gy/min) adjusted according to the published data and tumor growth condition [48, 49, 51] by a cobalt-60 unit (V-9, PICKER, USA). The distance from the radiation source to the skin of right thigh was 80 cm. A customized harness was used to immobilize the mice with only the right hind leg was exposed and the remainder of the body was shielded with five times the half-value thickness of lead [77].

2.2.3.4 Different treatment combinations of carboplatin and irradiation

doi:10.6342/NTU201704398

The total carboplatin dose was classified as low-dose (60 μg, 3 μg/g) and high-dose (300 μg, 15 μg/g) calculated by mouse body weight and adjusted according to the published studies [56, 78] as well as the feasible drug loading volume by mouse tumor size to explore the adequate carboplatin dose combined with RT. In order to compare the treatment effect of hydrogel carboplatin with aqueous carboplatin, the dose of hydrogel carboplatin was injected in a single dose, while the equal amount of aqueous carboplatin was divided into 3 doses and injected in 3 consecutive days. Hydrogel carboplatin or aqueous carboplatin was injected into the subcutaneous tumor by a syringe with a 28-gauge needle. The mice were categorized into the following groups according to their treatments: including shame (S), hydrogel (H), aqueous carboplatin (AC), hydrogel carboplatin (HC), RT (R), RT with hydrogel (HRT), RT with aqueous carboplatin (ACR), and RT with hydrogel carboplatin (HCR).

The purpose of the first-stage in vivo experiment was to investigate the synergistic effect of low-dose hydrogel carboplatin or aqueous carboplatin with RT. Mice were randomized into 5 treatment groups, including S, R, HRT, ACR, and HCR groups. The purpose of the second-stage in vivo experiment was to investigate the synergistic effects of high-dose hydrogel carboplatin or aqueous carboplatin with RT. Mice were randomized into 7 treatment groups, including S, H, AC, HC, R, ACR, and HCR groups.

Figure 8A and Figure 8B illustrated the cell number, dosage of hydrogel carboplatin and aqueous carboplatin, radiation dose, and schedules of drug delivery for first and second in vivo experiments, respectively [59]. The protocol of the second-stage experiment was modified according to the results of the first-stage experiment. The primary endpoint of the in vivo investigation was the tumor growth control effect according to different treatments. The secondary endpoints included survival and treatment-related local and systemic

doi:10.6342/NTU201704398

toxicities. The survival time was calculated from the day of tumor cell implant to the day of mice death or being sacrificed due to tumor dimension ≥ 20 mm or skin ulcer development. The treatment effects were compared among different treatment groups, especially between the single injection of hydrogel carboplatin and multiple injection of aqueous carboplatin.

2.2.3.5 Tumor growth evaluation by gross volume measurement and bioluminescence imaging (BLI)

The length and width of tumors were measured by an electronic caliper and the tumor volume was estimated by the formula: volume = 1/2 × length × width^2 [79]. Tumor volume was evaluated every 2 to 5 days according to the tumor growth condition. BLI was used for sequential tumor growth monitor [80]. Mice were anesthetized by isoflurance gas (8.6 mg/kg, respectively) and D-luciferin (0.2 mL) was injected intraperitoneally. BLI was acquired by spectrometer, In Vivo Image System (IVIS) SPECTRUM (exposure time: 30 sec; binning: medium; f/stop: 1) with Living Image® software (*PerkinElmer*), 10 minutes after D-luciferin injection with exposure for 30 seconds. BLI was evaluated every 5 to 8 days according to the tumor growth condition and facility availability [81]. The intensity of bioluminescence signal (expressed in radiance) from ALTS1C1-luc tumors and the maximum value was quantified by Living Image® software to estimate the tumor burdens [55].

2.2.3.6 Treatment effect evaluation by tumor gross and slice

doi:10.6342/NTU201704398

The gross tumors of different treatment combinations were dissected after mice being sacrificed, and slice with hematoxylin and eosin (H&E) stain was used to evaluate the histologic tumor cell proliferation and death.

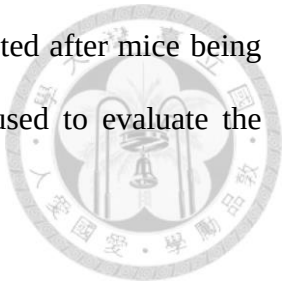

2.2.3.7 Toxicity evaluation by blood analysis and skin survey

Systemic toxicity of carboplatin was evaluated by the blood biochemistry study (BCS), including liver and kidney functions, and complete blood count (CBC), which were sampled 6 days after intratumoral injection of high-dose aqueous carboplatin [82]. The BCS and CBC were analyzed by ProCyte Dx® hematology analyzer (IDEXX, Maine, USA) and Cobas c111 analyzer (Roche, New Jersey, USA) respectively. Local toxicity of RT, such as skin ulcer, usually developing within 2 weeks after RT, was monitored sequentially up to 3 weeks after treatment.

2.2.4 Statistical analysis

Data analysis and statistical tests were performed using SPSS. OS was calculated on the basis of the date of tumor plant to the date of death or being sacrificed. Survival was calculated using the Kaplan-Meier product-limit method. Differences in survival were compared between the groups by using the log-rank test. Biocompatibility investigation of oxi-HA/ADH and tumor volume differences on a specific day among different treatment groups were analyzed by using one-way analysis of variance (ANOVA) or t-test according to the number of groups. All tests were two-sided and results with $p < 0.05$ were considered statistically significant.

doi:10.6342/NTU201704398

CHAPTER 3 RESULTS

3.1 Imaging biomarkers

3.1.1 Patient characteristics

We evaluated 145 patients whose glioblastoma was pathologically confirmed between August 2004 and December 2015. Three patients with active concomitant malignancies and six without post-CCRT neuroimaging were excluded. By December 2016, at a median follow-up period of 74.9 (range 47.7–102.1) months, 115 (84.6%) of the 136 patients had experienced disease progression, including tumor progression noted on imaging (107; 78.7%) and death (103; 75.7%); 33 patients survived without loss of follow-up [64]. Table 1 lists the patient characteristics, imaging findings, and treatment modalities [64]. A total of 132 patients (97.1%) underwent preoperative MRI and one underwent preoperative CT. Three patients with subtotal tumor resection were evaluated on the basis of postoperative CT or MRI findings before CCRT because of the unavailability of preoperative neuroimaging data.

3.1.2 Survival analyses

In the univariate analysis (Table 2) [64], the median OS was 19.7 and 28.6 months for patients with and without EPE, respectively ($p = 0.005$) (Figure 9, A1). PFS was 11.0 and 17.4 months for patients with and without EPE, respectively ($p = 0.011$) (Figure 9, A2). The median OS was 18.7 and 25.4 months for patients with and without sSVZCC invasion, respectively ($p = 0.021$) (Figure 9, B1). PFS was 10.7 and 14.6 months for patients with and without sSVZCC invasion, respectively ($p = 0.020$) (Figure 9, B2). In the multivariate analysis (Table 3), EPE was a significant adverse prognostic factor for OS and PFS (HR, 1.98; 95% CI, 1.28–3.05 and HR, 1.84; 95% CI, 1.23–2.76, respectively). sSVZCC invasion

doi:10.6342/NTU201704398

showed a near-significant trend for adverse OS (HR, 1.50; 95% CI, 0.96–2.34) and was a significant adverse prognostic factor for PFS (HR, 1.56; 95% CI, 1.03–2.38).

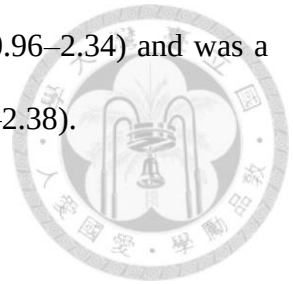

3.1.3 Progression pattern analysis

In the subgroup univariate analysis (Table 4) [64], the sSVZCC invasion status showed no significant differences for OS and PFS in either the EPE− or EPE+ groups. In the progression patterns analysis (Table 5) [64], EPE− patients without and with sSVZCC invasion were classified as Group I and Group II, respectively. The rates of EPD, local, regional, and distant progression were 2.8%, 58.3%, 2.8%, and 16.7% for Group I and 7.1% ($p = 0.486$), 71.4% ($p = 0.522$), 0% ($p = 1$), and 21.4% ($p = 0.697$) for Group II, respectively.

EPE+ patients without and with sSVZCC invasion were classified as Group III and Group IV, respectively. The rates of EPD, local, regional, and distant progression were 37.0%, 72.2%, 14.8%, and 22.2% for Group III and 71.9% ($p = 0.003$), 84.4% ($p = 0.291$), 56.3% ($p < 0.001$), and 34.4% ($p = 0.313$) for Group IV, respectively (Table 5) [64]. In EPE+/sSVZCC+ group, tumors with CCEPE were associated with a significantly higher rate of CCEPD than were those without CCEPE (77.8% vs. 20.0%, $p = 0.024$), whereas tumors with SVZEPE were associated with a significantly higher rate of SVZEPD than were those without SVZEPE (50.0% versus 6.3%, $p = 0.015$) (Table 5) [64].

During the period from 2004 to 2006, the 3-dimensional conformal radiation therapy (3DCRT) technique was given to patients who were scheduled for radiotherapy. With the advance in RT technologies, patients were treated mainly with the intensity-modulated radiation therapy (IMRT) technique and some with tomotherapy from 2007 to 2013, while the volumetric-modulated arc therapy (VMAT) technique was generally adopted after 2013.

doi:10.6342/NTU201704398

In our analysis, 21 (15.4%) patients received 3DCRT, 65 (47.8%) received IMRT, 42 (30.9%) received VMAT, and 8 (5.9%) received tomotherapy. Table 6 shows no significant difference in progression patterns in patients receiving 3DCRT compared with those receiving IMRT, VMAT, and tomotherapy techniques.

Figure 10 demonstrates distinct progression patterns and sites in 4 patients categorized according to the different combinations of SVZ and CC lesions [23]. A patient with synchronous SVZ (left occipital horn) and CC (left splenium) invasion before surgery presented no local progression (Figure 10, A1) but showed distant progression to the left cerebellum (Figure 10, A2) and regional progression of preoperative edematous areas to the contralateral hemisphere (Figure 10, A3). Another patient with synchronous SVZ (left frontal horn) and CC (left genu) invasion before surgery developed progression to the local tumor bed (Figure 10, B1) and left posterior CC along the occipital horn (Figure 10, B2). Figure 10C and 10D are the MRI images of 2 patients with local progression. One was diagnosed with SVZ invasion alone (left temporal horn) (Figure 10C) and the other had neither SVZ nor CC invasion (Figure 10D) before surgery [23].

Figure 11 demonstrates the distinct progression patterns observed after CCRT in 5 patients [64]. A patient with EPE−/sSVZCC− before surgery (Figure 11, A1,2) presented with local progression without EPD (Figure 11, A3). Another patient with EPE−/sSVZCC+ before surgery (Figure 11, B1,2) presented with local progression without EPD (Figure 11, B3). Figure 11, C1 and C2, describes a patient with EPE+/sSVZCC− before surgery, who presented with local progression with EPD (Figure 11, C3). Figure 11, D1 and D2, shows a patient with EPE+/sSVZCC+ and CCEPE before surgery, who presented with local progression with CCEPD (Figure 11, D3). Figure 11, E1 and E2, shows a patient with

doi:10.6342/NTU201704398

EPE+/sSVZCC+ and SVZEPE before surgery, who presented with local progression with SVZEPD (Figure 11, E3).

3.2 Intratumoral Hydrogel Carboplatin Injection

3.2.1 Biomaterial investigation

3.2.1.1 Characterization of oxi-HA/ADH hydrogel and hydrogel carboplatin by FTIR analysis

The FTIR spectrum (Figure 12A1) demonstrated the aldehyde functional group of oxi-HA at frequency 1730 cm^{-1} [59]. The spectrum peak at 1730 cm^{-1} of oxi-HA disappeared after mixing oxi-HA with ADH, which correlated to the consumption of aldehyde to form the imine bond between oxi-HA and ADH and suggested the hydrogel formation [54, 67]. The appearance of a new forming peak at 1528 cm^{-1} of oxi-HA/ADH was associated with the N—H function group of ADH [54, 67]. The appearance of a new forming peak at 545 cm^{-1} of oxi-HA/ADH hydrogel carboplatin (Figure 12A2) was associated with the Pt—N function group of hydrogel carboplatin [59, 83]. Our results are comparable with published study that the oxi-HA, ADH, and caboplatin compound into hydrogel carboplatin [54, 83].

3.2.1.2 Gelling time of oxi-HA/ADH hydrogel by rheometer

The rheological properties demonstrated that the gelation of oxi-HA/ADH started at temperature higher than 27.6 °C (Figure 13, A1) and the gelling time of oxi-HA/ADH from liquid state to gel state were 17 seconds at 37 °C (body temperature) (Figure 13, A2) [59].

doi:10.6342/NTU201704398

3.2.1.3 Degradation property of oxi-HA/ADH hydrogel

At 72 and 120 h, degradation percentages for oxi-HA/ADH (Figure 14) were 5.2% and 18.2%, respectively, which means less than 10% hydrogel was degraded within the first 3 days and more than 20% hydrogel started to degrade after 5 days [59]. The slow degradation property of oxi-HA/ADH hydrogel provides a stable carrier to load drug.

3.2.1.4 Drug release of hydrogel carboplatin by ICP-MS

Figure 15 demonstrates the cumulative release profile of carboplatin from oxi-HA/ADH hydrogel [59]. The ICP-MS result demonstrates two phases of the carboplatin release from hydrogel, including a burst release of 63.7% during the first 24 h, followed by a steady release of 16.6% over the 24 to 96 h. The drug release profile of carboplatin hydrogel illustrated that carboplatin was released up to 80.3% in 96 h, which provide 4 days to combine with RT after drug injection.

3.2.2 In vitro investigation

3.2.2.1 Biocompatibility of hydrogel

The WST-1 analysis (Figure 16A) demonstrated the cell viability of 3T3 cells cultured in oxi-HA/ADH hydrogel extraction medium was not significantly different compared with those in the control and negative control groups (p = 0.644) [59]. The LDH assay (Figure 16B) indicated the cytotoxicity oxi-HA/ADH is not significantly different from the negative control group (p = 0.173) [59].

doi:10.6342/NTU201704398

The Live/Death staining (Figure 17) illustrated that nearly all the 3T3 cells were viable in the oxi-HA/ADH hydrogel after 3 days' cultivation [59]. Our results, including WST-1 analysis, LDH assay, and Live/Death staining, demonstrated no evidence of toxicity of oxi-HA/ADH hydrogel, which is comparable with the published data [54].

3.2.2.2 IC_{50} of carboplatin to ALCS1C1 cells

The IC_{50} (Figure 18) test demonstrated that the in vitro concentrations of carboplatin to inhibit 50% ALCS1C1 cells to proliferation was 44.4 and 18.5 μg/mL after 1-day and 3-day treatment, respectively [59]. Considering the IC_{50} of carboplatin to AL1SC1 cells, drug carrying ability of hydrogel, and published data of Intratumoral carboplatin injection the adequate carboplatin concentration for in vivo experiment, we adopted the carboplatin concentration of 2 mg/mL for our in vivo investigation [56, 78].

3.2.3 In vivo investigation

3.3.1 First-stage in vivo experiment (low-dose carboplatin)

Five treatment groups, including S (N = 5), R (N = 5), HRT (N = 5), ACR (N = 5), and HCR (N = 5), were analyzed in the first-stage in vivo experiment. One mouse in HRT group and and 2 mice in HCR group died early due to the anesthesia procedure.

Comparing with the sham group, the BLI (Figure 19) demonstrated the relatively delayed tumor progression in all treatment groups [59]. Correspondingly, the tumor volume curves (Figure 20) of the treatment groups demonstrated tumor progression after temporary

doi:10.6342/NTU201704398

tumor control effects [59]. On day 24, the tumor volume analysis (excepting sham group) by one-way ANOVA showed no difference of tumor progression for RT with and without low-dose carboplatin (p = 0.787). The survival data (Table 7) revealed that all mice treated with RT alone or combined with low-dose carboplatin died within 39 days after tumor implant [59].

3.2.3.2 Second-stage in vivo experiment (high-dose carboplatin)

Seven treatment groups, including S (N = 7), H (N = 9), AC (N = 9), HC (N = 9), R (N = 6), ACR (N = 6), and HCR (N = 6), were analyzed in the second-stage in vivo experiment. The BLI (Figure 21) demonstrated the tumor nearly complete response in HCR and ACR groups, while tumor progression in other treatment groups [59]. The bioluminescence signal represented in radiance showed corresponding findings (Figure 22) [59].

Figure 23 [59] illustrates the tumor volume curves of different treatment modalities combination in the second-stage in vivo experiment with high-dose carboplatin (15 μg/g), including RT, aqueous carboplatin (100 μg once daily for 3 days) or hydrogel carboplatin (300 μg in a single dose on the first treatment day) alone, and combining RT with aqueous or hydrogel carboplatin, respectively. In ACR and HCR groups, the tumor volume curves demonstrate good tumor control without difference (p = 0.904), while R group demonstrates tumor progression after temporal tumor volume control and AC and HC groups demonstrate persistent tumor progression. Tumor injected with hydrogel alone showed the same tumor growth as those without any treatment.

doi:10.6342/NTU201704398

The subgroup tumor volume analysis on day 24 by t-test demonstrated no significant difference of tumor control effects by comparing ACR with HCR group (p = 0.904) and AC with HC groups (p = 0.747), respectively. HCR group showed better tumor control than either RT group (p = 0.007) or the HC group (p = 0.006) [59].

Table 8 lists the survival time according to different treatment modality combinations in the second-stage [59]. Three mice in HCR group and 4 mice in ACR group had no tumor recurrence after treatment on day 104 after tumor implant. The survival curves (Figure 24) revealed that the HCR and ACR groups had 104-day survival rates of 50% and 66.7% without significant difference (p = 0.648). Other mice treated with radiation or high-dose carboplatin alone died within 40 days after tumor implant.

Figure 25A demonstrated the tumor cross section after intratumoral injection with oxi-HA/ADH hydrogel dye [59]. The blue area illustrated the diameters of dye distribution 1 day and 3 days after hydrogel dye injection were 7 and 9 mm, respectively. Our results suggested the intratumoral drug injection provides adequate drug distribution to cover the tumor area. The response of different treatment combinations evaluated by slices of H&E stain were illustrated in Figure 25, B1 to B3 and C1 to C4, respectively [59]. The H&E stain of tumor receiving RT (Figure 25, B1) showed both cell death (yellow rectangular area at 100× and yellow arrow at 400×) and tumor cell proliferation (red rectangular area at 100× and red arrow at 400×). The H&E stain of tumor receiving either aqueous carboplatin with RT (Figure 25, B2) or hydrogel carboplatin with RT (Figure 25, B3) showed prominent cell death. Contrastingly, H&E stain of tumor cell growth under no treatment (Figure 25, C1) and injection of hydrogel (Figure 25, C2), aqueous carboplatin (Figure 25, C3), and hydrogel carboplatin (Figure 25, C4) all showed tumor cell proliferation only.

doi:10.6342/NTU201704398

Table 9 illustrated the blood analysis, and no neutropenia and renal or hepatic function impairments were detected [59]. Figure 26A demonstrated transitory weight loss in HCR and ACR of high-dose carboplatin treatment groups then recovered without death [59]. Figure 26, B1 and B2, demonstrated that no drug injection or RT-related skin ulcer was observed in 3 weeks in HCR and ACR treatment groups, respectively [59].

CHAPTER 4 DISCUSSION

4.1 Imaging Biomarkers and Clinical Impacts

4.1.1 Disease classification and RT strategies

Figure 27 presents the data processing workflow of our study [64]. We used the index of EPD, which involved tumors continuously extending or discretely migrating along the PE ≥ 2 cm from the preoperative tumor margin, to investigate the tumor extension or migration ability relative to the EORTC delineation dimensions. Our study results demonstrate that EPE and sSVZCC invasion determined poor OS and PFS, and combining these two factors led to the identification of specific progression patterns. The low EPD rate in the EPE− patients suggests that the delineation dimension of a tumor bed with a 2-cm margin is sufficient to cover the tumor progression area in these two patient groups. In contrast, the EPE+/sSVZCC− and EPE+/sSVZCC+ patients had high EPD rates, which suggests that the delineation dimension of a tumor bed with a 2-cm margin is insufficient to cover the tumor progression area in these two patient groups.

Our results provide statistical evidence for the individualized delineation of RT targets. Group I and II (confined type) glioblastomas were highly associated tumor progression

doi:10.6342/NTU201704398

within 2 cm of the preoperative tumor margin, which corresponds to the EORTC target delineation guidelines [20], without specifically including the preoperative edematous area. The EPD rate for the Group III patients was 37.0%, which requires RTOG target delineation [20] to cover the potential tumor progression at the preoperative edematous area. The Group IV patients had an EPD rate of 71.9%, which suggests that comprehensive target delineation including the tumor bed and PE is necessary. Some studies reported the target volume differences between biological tumor volume (BTV) on positron emission tomography and gadolinium-enhanced tumor volume on MRI scan in glioblastomas [84, 85]. Nevertheless, the association between PE and BTV remains uncertain and requires further investigation.

The distinct progression patterns associated with specific survivals in the different groups indicate that individualized treatment strategies are required. In Groups I and II, most tumor progressions developed within a 2-cm margin of the preoperative tumor; thus, enhanced local treatments, such as hypofractionated RT [86, 87] and BCNU wafer [35], were required. Reddy et al. demonstrated that hypofractionated RT with temozolomide reduced the local progression pattern [86]. Iuchi et al. reported that hypofractionated high-dose RT with concurrent and adjuvant temozolomide altered the dominant failure pattern from localized to disseminated disease and prolonged the survival of glioblastoma patients [87]. The Group I and II patients with predominant local tumor progression within 2 cm of the preoperative tumor margin were considered as candidates for BCNU wafer implantation [35].

In the Group III (intermediate type) patients, the EPD rate was 37.0% under an RT dosage of 46 Gy in 23 fractions, which suggests that a higher dose should be prescribed for PE in order to increase tumor control at the area. Farzin et al. revealed that the simultaneous integrated boost (SIB) method offers advantages over the sequential boost method in sparing

doi:10.6342/NTU201704398

organs at risk [88]. A phase I study by Truc et al. demonstrated that SIB RT use was feasible for increasing the dose to the tumor bed and PE [89]. SIB RT is an option for escalating the dose to PE in Group III patients.

In the Group IV (extensive type) patients, the EPD rate was 71.9%, and the rate of discrete tumor progression at PE areas was 56.3%. The high progression rate associated with PE corresponds with that described in a review study by Jansen et al., who demonstrated glioblastoma cells at PE areas on CT and MRI scans [21]. In patients with sSVZCC invasion and CCEPE or SVZEPE, the associated CCEPD and SVZEPD rates were 77.8% and 50%, respectively, which suggests that tumor extension or migration is highly correlated with CCEPE or SVZEPE. Our results demonstrate that an RT dosage of 46 Gy in 23 fractions to PE is insufficient for tumor control, and that comprehensive delineation including the tumor bed and PE—especially CCEPE or SVZEPE—for high-dose RT is required to increase tumor control.

Some studies have explored the association between radiation dose irradiation of SVZ or CC and clinical outcome of glioblastoma [90, 91]. Chen et al demonstrated that among glioblastoma patients with gross total resection, a mean ipsilateral SVZ dose of 40 Gy or greater was associated with a significantly improved PFS compared with those receiving less (15.1 vs 10.3 months; $p = 0.028$) [90]. The cerebral falx represents a boundary for migrating tumor cells, whereas the CC provides a route for the tumor to spread to the contralateral hemisphere [92]. Unkelbach et al proposed a tumor growth model that provided a method to account for anisotropic growth patterns of glioma and the migration of tumor cells through the CC in radiotherapy planning [92]. Correspondingly, through the analysis of progression patterns and sites, our previous study (Figure 27) significantly identified the specific areas of

doi:10.6342/NTU201704398

progression for glioblastoma with sSVZCC invasion: the CC (61.1%), bilateral hemispheres (47.2%), preoperative edema area (41.7%), and ventricles (38.9%) [23]. For tumors with sSVZCC invasion, the PE areas were prevalent progression sites, especially for the edema extending through the CC to the contralateral hemisphere, as presented in Figure 3, A3. We also found that for patients with sSVZCC invasion, virtually all ventricular progression occurred at the frontal and occipital horns [23]. These specific progression areas are potential radiotherapy targets for patients with sSVZCC invasion.

4.1.2 High-dose proton boost for confined type glioblastoma

High-dose proton boost to tumor bed was investigated for local control of glioblastoma [93]. In the further analysis by PE extent, glioblastoma patients of PE ≤ 19 mm compared with those > 19 mm showed better OS after high-dose proton boost to tumor bed (42.4 versus 18.4 months, $p = 0.023$) [94]. For patients with PE ≤ 19 mm, 92% tumor progression developed within 19 mm from the tumor margin. The 3-year local control rate was 38% [94]. These results suggested that intensive local treatment improves the disease control and OS for glioblastoma with relative small PE.

4.1.3 Disease classification and other treatment strategy

Wang et al. demonstrated high vascular endothelial growth factor (VEGF) expression levels with a peritumor edema extent of > 2 cm in glioblastoma [95]. Takano et al. described that the antiedema effect of bevacizumab, a monoclonal antibody that blocks angiogenesis by inhibiting VEGF, administered for the treatment of recurrent glioblastoma was marked and prolonged at 6 months [96]. The efficacy of additional bevacizumab for enhancing tumor

doi:10.6342/NTU201704398

control at the edematous area in Group IV patients requires further investigation.

Accumulating evidence suggests that the stem cell markers, CD133 and CD44, indicate molecular subtypes in glioblastoma. In the study of Brown et al., coexpression analysis of CD133 and CD44 identified proneural and mesenchymal subtypes of glioblastoma. Patients with CD133 coexpression module signature (CD133-M) had significantly improved survival from radiotherapy treatment but no significant benefit from temozolomide [97]. In contrast, patients with CD44-M had higher survival benefit from temozolomide treatment but lower benefit from radiotherapy, compared to CD133-M patients [97]. In the study of Piccirillo et al., they observed that for glioblastoma tissues of the same patients, the tumor cells derived from the part of sub-ependymal zone were more resistant to supra-maximal chemotherapy doses of different drugs than tumor cells outside the zone [98], which suggests more intensive drug therapies are required when glioblastoma involving the SVZ.

Chaichana et al reported that patients with butterfly glioblastoma had poor prognosis but nevertheless benefited from aggressive treatments including debulking surgery, maximal safe surgical resection, temozolomide chemotherapy, and radiotherapy [31]. Glioblastoma with sSVZCC invasion is considered an early stage of butterfly glioblastoma and therefore may also benefit from comprehensive treatment strategies. For those with and without sSVZCC invasion, our study significantly determined the different prognosis and distinct progression areas, specifically at the CC, bilateral hemispheres, preoperative edema, and lateral ventricles [23]. These results imply that the therapeutic approach to patients with sSVZCC should be different from that for patients without invasion.

4.1.4 Imaging biomarkers and molecular biology

doi:10.6342/NTU201704398

Because our IDH1 data were only available for 24 patients with one presenting mutated type, further analysis could not be performed. Wang et al. reported that in patients with the IDH1 mutation, ring-like tumor contrast enhancement and peritumoral edema (> 1 cm) indicated shorter PFS and OS [99]. Another limitation of our study is that we could not analyze the prognosis or progression patterns of MGMT promotor methylation status because of the lack of data. According to Carrillo et al., edema levels determined survival in methylated but not unmethylated tumors, meaning that patients with MGMT promotor methylation and peritumor edema of < 1 cm had favorable OS [100].

Our previous study demonstrated that the tumor progression rates at PE areas are > 40% and < 10% for those with and without sSVZCC invasion, respectively [23]. The high progression rates at the CC and bilateral hemispheres for glioblastoma with sSVZCC suggest the potential correlation between glioblastoma stem cells and interhemispheric connections of cerebral commissures [23]. In the same study, all 3 patients with combined invasion of lateral ventricles and anterior commissure in our study exhibited progression patterns at the bilateral hemispheres that were comparable with those having sSVZCC invasion [23]. Kakita et al reported that in the neonatal rat model, progenitors within the SVZ at the angle of the lateral ventricle appeared to move in an undirected manner; however, after migration, they extensively moved radially and tangentially in the ipsilateral hemisphere of the injection side. They also proposed that the progenitors migrate along the unmyelinated axon fiber fascicles in the CC [101], which corresponds to the progression sites of our patients with sSVZCC invasion. In the adult mammalian brain, neural progenitor cells are present and neurogenesis occurs in the SVZ on the walls of the lateral ventricles [36-38]. The migration of glial progenitors depends on their contact with the cerebral commissures, as demonstrated in a

doi:10.6342/NTU201704398

study on neonatal rats [102]. The high rates of progression to the CC and bilateral hemispheres suggests that the migration of glial progenitors depends on their contact with NFTs [23]. These findings indicate the potential interactions between glioblastoma stem cells and the CC.

4.2 Treatment Impact and Clinical Application of Hydrogel Carboplatin

Through the comprehensive study design, we integrated the biomaterial, in vitro, and in vivo investigations to propose a novel combination of carboplatin with hydrogel and surveyed its optimized treatment combining with RT for glioma. According to the analyses of drug release profile, biocompatibility, tumor control, survival, and side effects in this study, we demonstrated hydrogel carboplatin as an effective, simplified, and safe modality for local drug delivery to combine with RT for treating mice glioma, which provides a further clinical application for brain tumor treatment.

4.2.1 Effectiveness of hydrogel carboplatin combined with RT for tumor control

We demonstrated that the hydrogel dye diffused 7 to 9 mm from the injection site after intratumoral injection, which provides adequate distribution extent of hydrogel carboplatin in brain tumors after excision clinically. Regarding to the carboplatin dose, we used different dosages of carboplatin combined with RT to investigate the synergistic treatment effect. In the first-stage in vivo experiment using low-dose carboplatin (3 μg/g), the tumor control effect of ACR and HCR treatment groups was not different from R treatment group, which suggests low-dose carboplatin is not sufficient for tumor control. In the second-stage in vivo

doi:10.6342/NTU201704398

experiment using high-dose carboplatin (15 μg/g), the tumor control effect and survival of both HCR and ACR treatment groups were significantly better than R, HC and AC treatment groups. We designed the timing of RT on the second and third days after hydrogel carboplatin injection according to the drug release profile of hydrogel carboplatin and the tumor growth course of mice to maximize the CCRT synergistic effect. The tumor control effect of high-dose CCRT resulted in the higher complete response rate and longer survival time than carboplatin or RT alone. These results demonstrated that the synergistic effect of combining high-dose carboplatin with RT is more robust than RT or carboplatin alone. Clinically, most malignant gliomas progress or recur at the surgical cavity after tumor excision and RT [16-18]. Considering the clinical demand and our study results, the local delivery of hydrogel carboplatin at surgical cavity combined with RT is an effective treatment for malignant gliomas.

4.2.2 Convenience of hydrogel carboplatin administration to combine with RT

The administration of drug by thermogelling hydrogel carrier provides a different drug delivery option compared with wafer implant and aqueous drug via CED implant during surgery. The hydrogel form presents better conformal ability compared with wafer, and better attachment compared with aqueous form [42]. Our results indicates that once oxi-HA/ADH carboplatin was injected into in vivo condition at 37 °C, oxi-HA/ADH carboplatin formed gel in 17 seconds [67]. This gelling time of oxi-HA/ADH carboplatin is adequate for intratumoral injection and hydrogel stabilization for mice subcutaneous tumor model. For human brain tumor application, longer drug gelling time is required, which can be achieved

doi:10.6342/NTU201704398

by increasing the concentration of ADH in the hydrogel, ranging from 2 to 3 min at 37 °C [54]. The thermogelation (thermal-dependent gelling) characteristic provides adequate time for drug injection and stabilization [68], which makes hydrogel carboplatin more adaptable to the shape of surgical cavity, easier adhesion to the tissue, and full coverage of surgical cavity compared with wafer-form and aqueous drugs [42].

Our results of low-dose and high-dose carboplatin experiments indicated that the synergistic effect with RT requires sufficient carboplatin dose. To maintain the adequate carboplatin dose takes drug via CED with daily infusion [49, 51] or slow release via drug carrier, including wafer [41] or hydrogel [55-58]. The clinical use of CED or wafer is limited due to its inconvenience and potential side effects [42, 52, 53]. Using the features of slow and steady release of hydrogel and synergistic effect of carboplatin with RT [46, 47], we compounded and applied the hydrogel carboplatin to treat the mice glioma. By comparing the effects of single injection of hydrogel carboplatin with multiple injection of aqueous carboplatin to investigate the feasibility and convenience of hydrogel carboplatin. Comparing the HC verse AC and HCR versus ACR groups respectively of the second-stage in vivo experiment, the tumor control effects and survivals of single dose hydrogel carboplatin (300 μg) were comparable with the aqueous carboplatin with daily dose (100 μg) for 3 days. The results indicate that the single injection of hydrogel carboplatin facilitates the drug administration without compromising the anti-tumor effect. When combining with RT, the single injection of hydrogel carboplatin simplified the concurrent RT course without compromising the synergistic effects.

One published study using covalent linking of platinum and hydrogel to compose hydrogel polymer–platinum, which made the platinum release lasted more than 60 days [68].

doi:10.6342/NTU201704398

Clinically, the RT course duration for malignant glioma ranges from 3 to 6 weeks and hydrogel carboplatin is feasible for single injection during surgery rather than daily local infusion via CED. The degradation time of hydrogel ranges from 4 to 6 weeks after injection [67], which avoids interfering the neuroimaging follow-up in 8 to 12 weeks after treatment competed. Our results and published data indicates that using local and single injection of hydrogel carboplatin to combine with RT is a feasible treatment modality for malignant glioma [68, 70].

4.2.3 Safety of hydrogel carboplatin with RT

According to our in vitro study, the WST-1, LDH test, and LIVE/DEAD staining validated the biocompatibility of oxi-HA/ADH hydrogel. In the first-stage in vivo experiment, the tumor growth curves of R and HRT groups showed no significant difference, which suggests no additional toxicity of hydrogel when combining RT. In the second-stage in vivo experiment, through the white blood count, and renal and liver function tests, no systemic side effect was detected under the high-dose (15 μg/g) of either hydrogel carboplatin single dose or aqueous carboplatin daily injection for 3 days. In all treatment groups, no drug injection, radiation or CCRT-related skin ulcers were observed and the transitory weight loss was acceptable.

Due to the size scale of mice, the total drug dose for single injection was limited. Comparing with human brain, the drug dose loaded by hydrogel is able to be higher. According to the mice tumor growth schedule, we design the total drug release in 4 days and RT on the second and third days after first drug dose injection. The drug release time can be

doi:10.6342/NTU201704398

prolonged up to 5 weeks technically [54] to fit the clinical CCRT course for malignant gliomas. In order to measure the tumor volume serially, we adopted the subcutaneous implant model rather than brain implant model. Our results demonstrated the intratumoral drug delivery, but the effect to normal brain tissue or its tolerance dose requires further investigation. The influences on tumor growth and treatment effect resulting from the environment differences between subcutaneous tissue and brain needs more survey.

CHAPTER 5 CONCLUSIONS AND FUTURE PROSPECT

5.1 Clinical Investigation

In the clinical investigation of this study, we analyzed the associations between these imaging factors and survival and tumor progression patterns and rates after CCRT and proposed corresponding RT target volume delineations and dose prescriptions. Our study demonstrated that EPE and sSVZCC invasion are highly associated with glioblastomas spreading extent and routes. The two imaging biomarkers provide clinical indexes to classify glioblastoma patients into different groups and in radiotherapy decision-making for individual patients, which introduces potential clinical investigation topics for the future.

5.2 Basic Investigation

In basic investigation of this study, we compounded a novel drug combination of thermogelling hydrogel carboplatin to satisfy the unmet clinical need for glioma treatment. Through the comprehensive biomaterial, cell, and animal experiment design, we significantly demonstrated that thermogelling hydrogel carboplatin simplified the drug delivery method

doi:10.6342/NTU201704398

and frequency without compromising the synergistic effect with RT, which makes intraoperative single drug injection followed by RT a feasible and potential clinical treatment. We chose carboplatin with well-established CCRT effects and hydrogel with well-accepted biocompatible features as a novel drug delivery combination, which helps accelerate the application process for further clinical trials. The impact of our study results is that we significantly demonstrated intratumoral injection of hydrogel carboplatin with RT as an effective, convenient, and safe treatment combination for malignant gliomas which is potential for clinical application.

doi:10.6342/NTU201704398

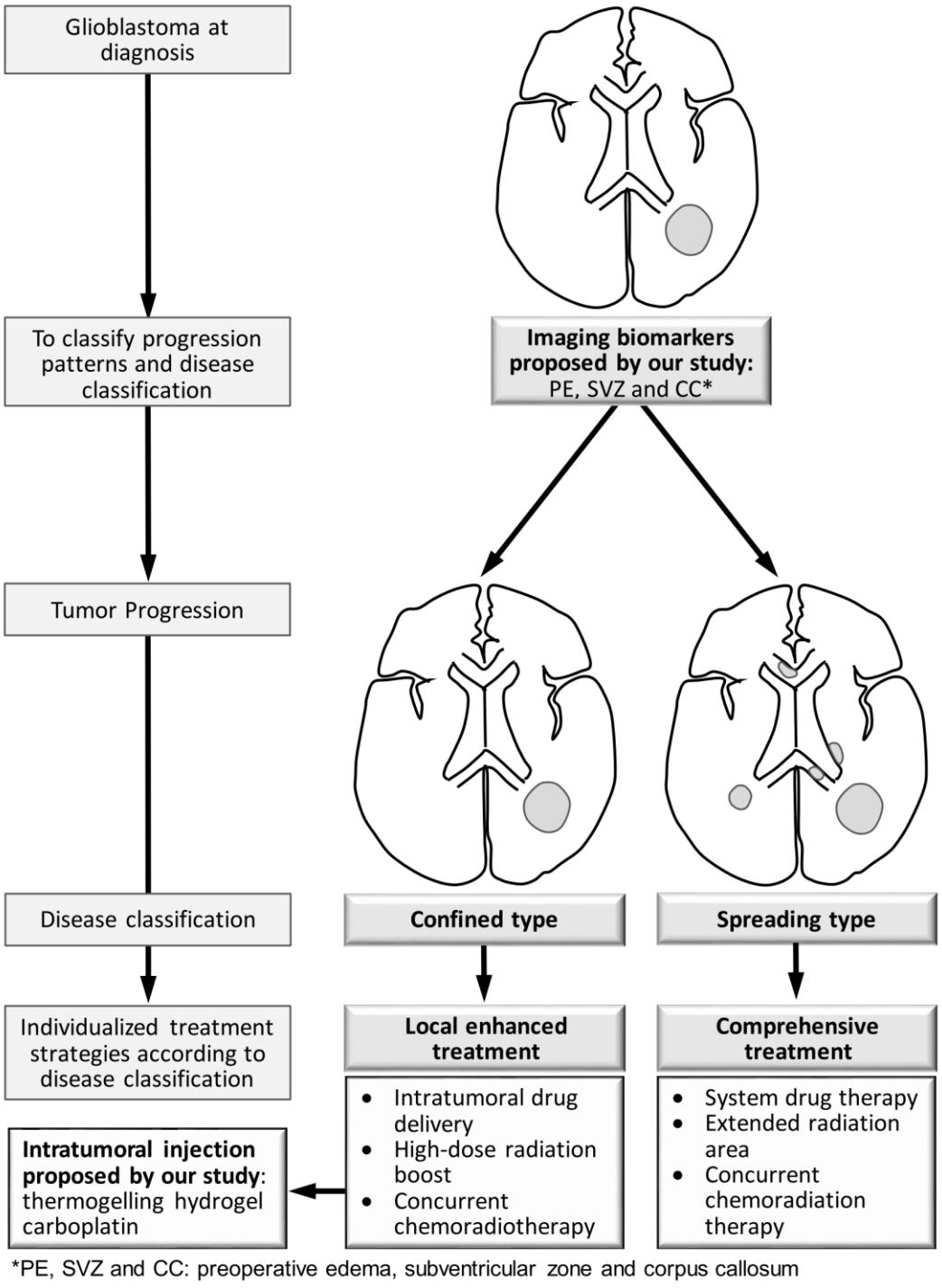

Figure 1. **The clinical and basic research perspectives of our glioblastoma study**. We proposed a comprehensive study, including imaging analysis and drug delivery investigation, to satisfy the clinical unmet needs for glioblastoma treatment.

doi:10.6342/NTU201704398

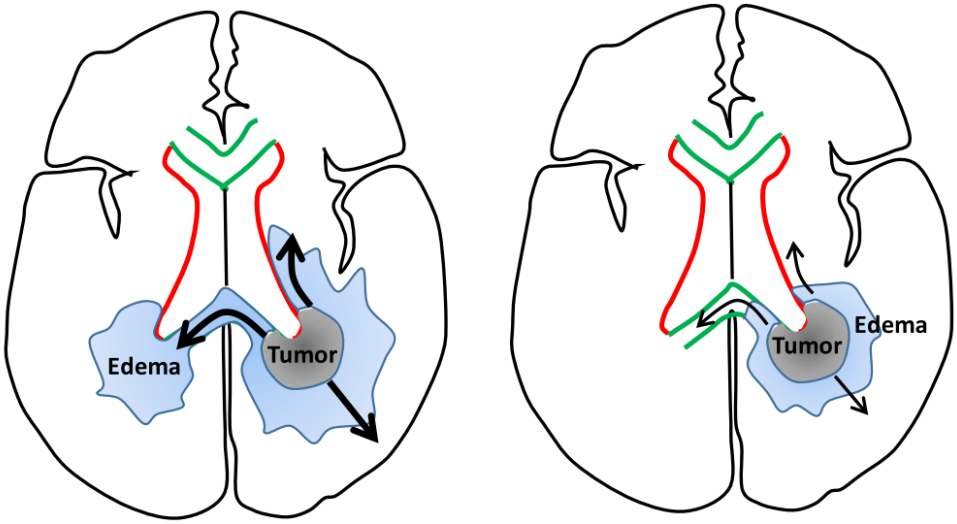

Figure 2. **The correlation between tumor location with edema and tumor migration**. The interactions between the anatomical factor subventricular zone (red line) and corpus callosum (green line) the pathophysiological factor preoperative edema (blue color wash) and the associated clinical impacts, including tumor migration ability and directions (black line with arrow) [64].

doi:10.6342/NTU201704398

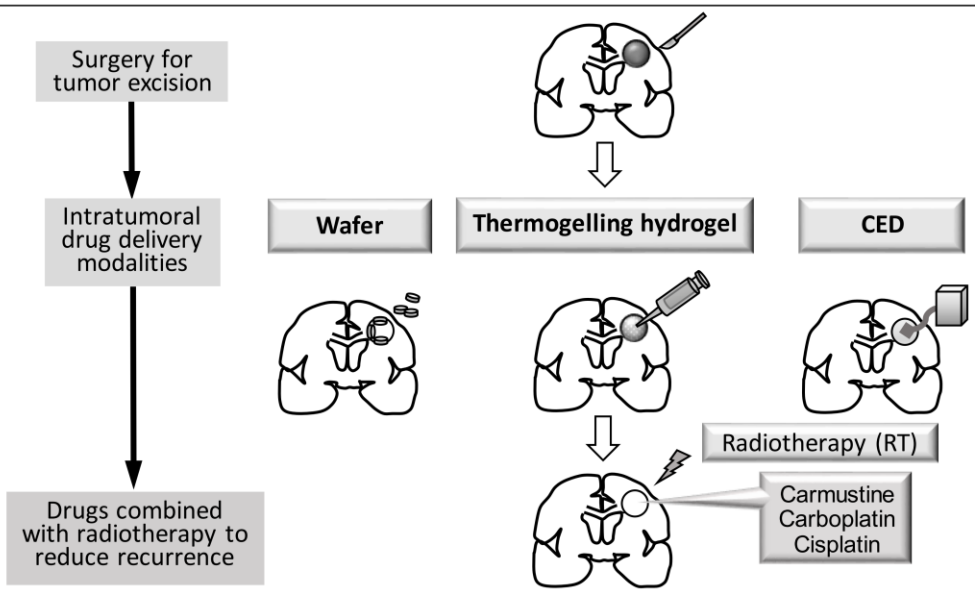

Comparison of Characteristics Among Different Delivery Modalities and Drugs

Drug carrier/device	Wafer	Thermogelling hydrogel	Convection enhanced delivery (CED)
Convenience			
Clinical usage	Not regularly used	Under investigation	Rarely used
Drug form	Solid	Gel	Liquid
Drug conformity	Inferior	Superior	Superior
Drug-tissue adhesion	Inferior	Superior	Inferior
Drug delivery method	Implant	Injection	Infusion
Thermogelation	No	Yes	No
Drug release duration	1 to 5 days [41]	1 to 60 days [66]	About 1 day [33]
Delivery frequency	Single	Single	Multiple
With 3- to 6-week RT	Infeasible	Feasible	Infeasible
Safety			
Backflow risk	No	No	Yes [53]
Degradation time	6 to 8 weeks [41]	4 to 6 weeks [54]	Not applicable
Drug type	**Carmustine**	**Carboplatin**	**Cisplatin**
Effectiveness			
Radiosensitization	Low [59]	High [47]	Intermediate [47]
Novel combination proposed in the study		**Thermogelling hydrogel carboplatin**	

Figure 3. **The rationale and purpose in the current basic study**: by comparing the characteristics of the intratumoral delivery modalities and drugs for malignant gliomas to propose a novel combination to satisfy the unmet clinical need [59].

doi:10.6342/NTU201704398

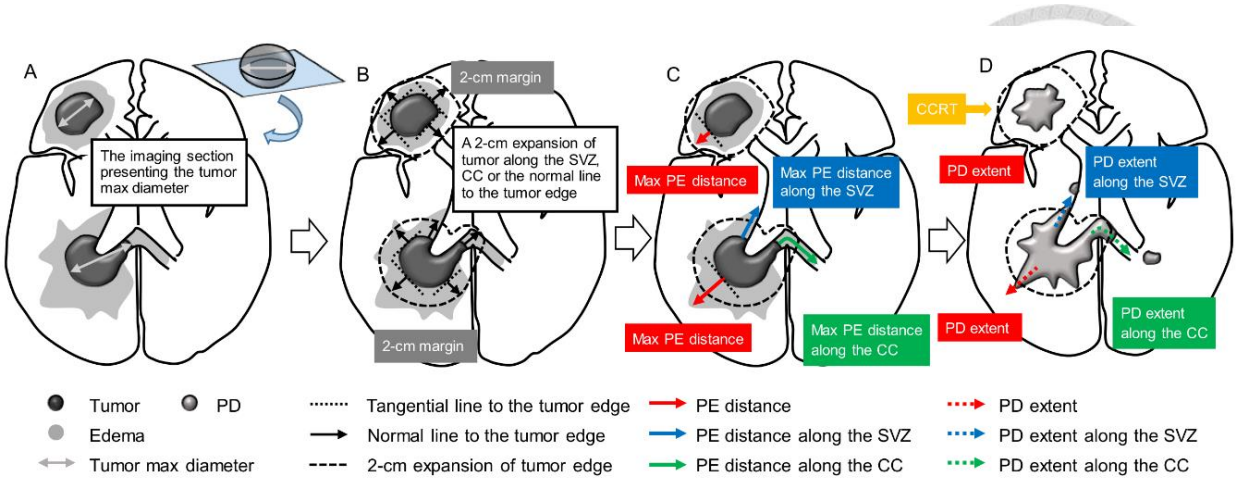

Figure 4. **The method of evaluating the preoperative edema extent in our clinical study**. (A) Select the image section that presents the maximum diameter of preoperative tumor. (B) Create a 2-cm expansion of tumor edge along SVZ (the lateral wall of lateral ventricles) or CC if these structures are invaded. Otherwise, draw tangential lines to the tumor edge and then use their normal lines to expand a 2-cm margin of the tumor edge. (C) Use the 2-cm expansion margin of tumor edge as a reference boundary to evaluate the PE extent. (D) Apply the 2-cm expansion margin of the preoperative tumor edge on the similar image sections after CCRT to evaluate the PD extent [64].

doi:10.6342/NTU201704398

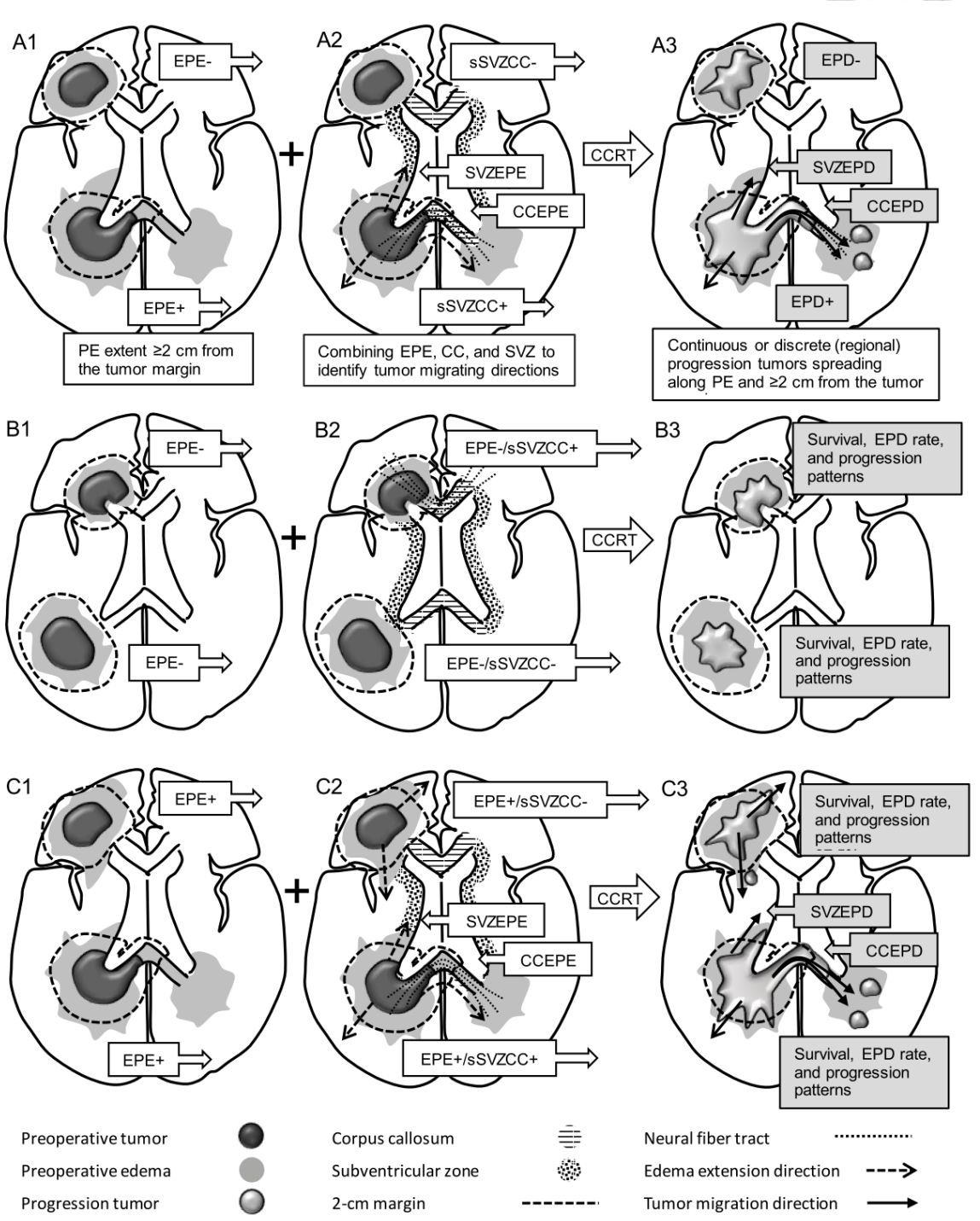

Figure 5. **The definitions of edema extent and progression patterns**. (A) Illustrations of (A1) EPE (PE ≥ 2 cm from the tumor margin) combined with (A2) sSVZCC invasion to evaluate the rates of EPD (continuous or discrete progression of tumors spreading along the

doi:10.6342/NTU201704398

PE areas and > 2 cm from the tumor margin), (A3) SVZEPD, and CCEPD after CCRT. (B) Illustrations of (B1) EPE− and (B2) sSVZCC+/− invasion to evaluate the rate of (B3) EPD after CCRT. (C) Illustrations of (C1) EPE+ and (C2) sSVZCC+/− invasion to evaluate the rates of (C3) EPD, SVZEPD, and CCEPD [64].

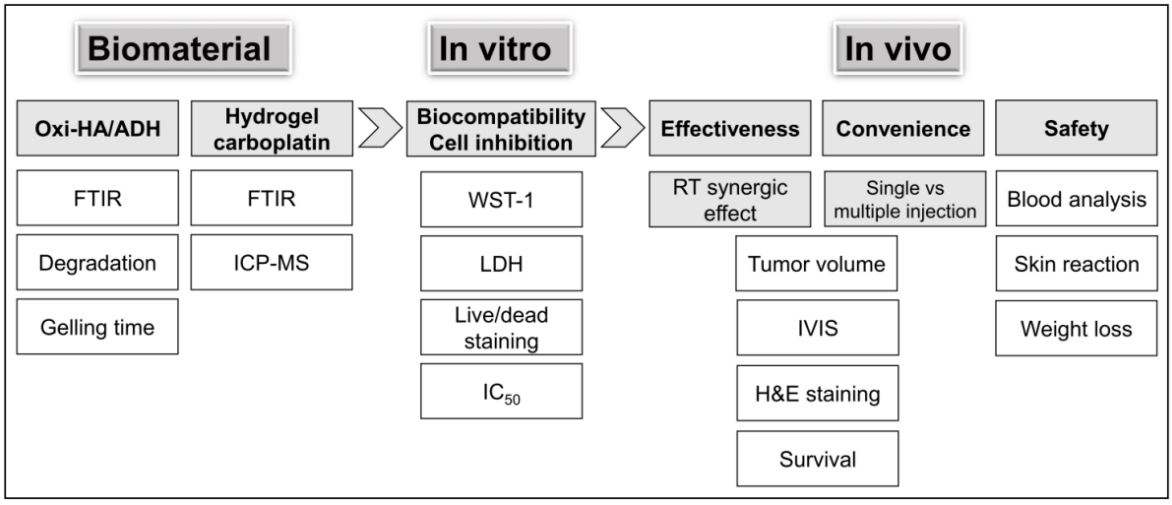

Figure 6. **The workflow of our basic study design**: biomaterial, in vitro, and in vivo investigations [59].

doi:10.6342/NTU201704398

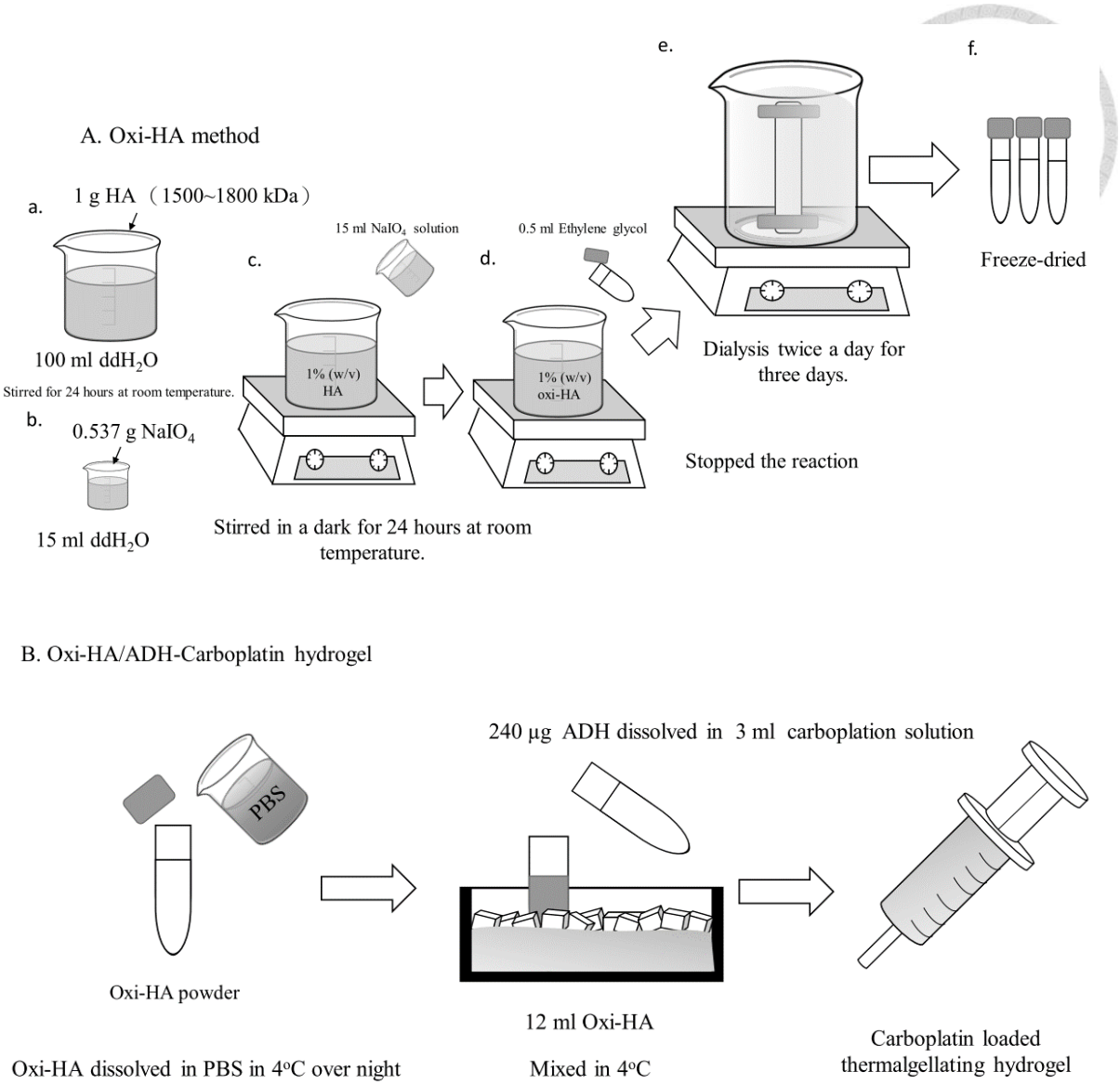

Figure 7. **Drug preparation**: the procedures of (A) oxi-HA/ADH hydrogel and (B) hydrogel carboplatin preparation. (Figures courtesy of Xue-Shi Lai, MSc.)

doi:10.6342/NTU201704398

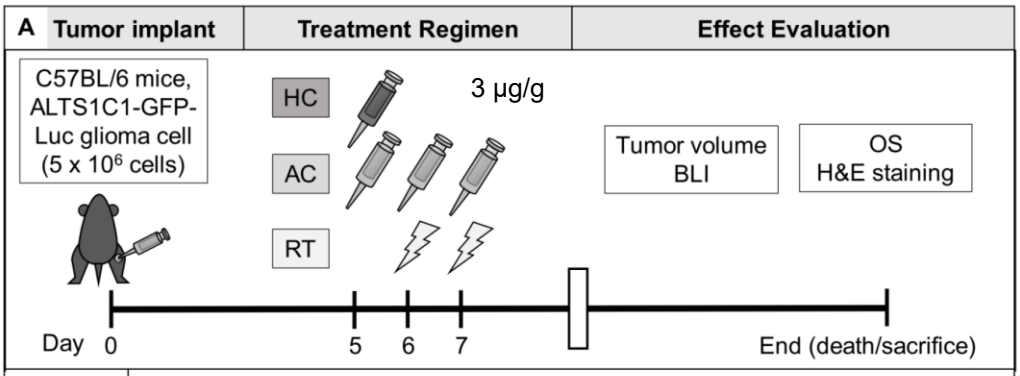

Group	Treatment Regimen
I-S	Saline (10 μL x 3 days)
I-R	Saline (10 μL x 3 days) + Radiotherapy (10 Gy/day x 2 days)
I-HR	Hydrogel (30 μL) + Radiotherapy (10 Gy/day x 2 days)
I-ACR	Aqueous carboplatin (20 μg/10 μL x 3 days) + Radiotherapy (10 Gy/day x 2 days)
I-HCR	Hydrogel carboplatin (60 μg/30 μL) + Radiotherapy (10 Gy/day x 2 days)

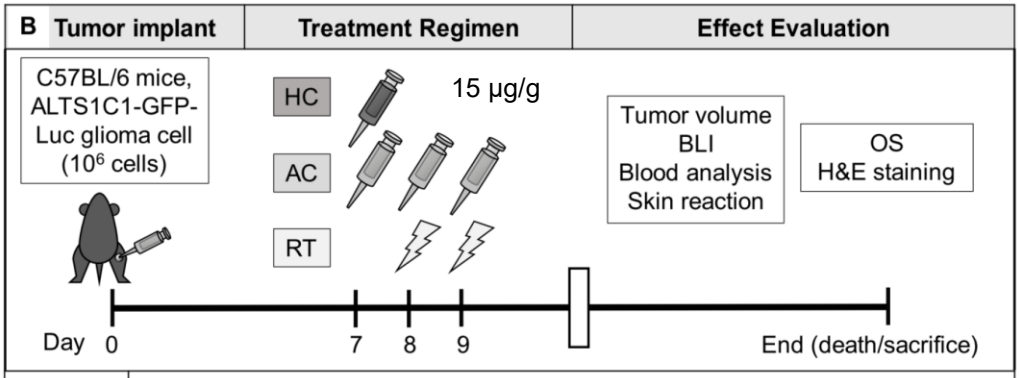

Group	Treatment Regimen
II-S	Saline (50 μL x 3 days)
II-H	Hydrogel (150 μL)
II-AC	Aqueous carboplatin (100 μg/50 μL x 3 days)
II-HC	Hydrogel carboplatin (300 μg/150 μL)
II-R	Saline (50 μL x 3 days) + Radiotherapy (10 Gy/day x 2 days)
II-ACR	Aqueous carboplatin (100 μg/50 μL x 3 days) + Radiotherapy (10 Gy/day x 2 days)
II-HCR	Hydrogel carboplatin (300 μg/150 μL) + Radiotherapy (10 Gy/day x 2 days)

Figure 8. **The treatment regimens and evaluation protocol of our mice study**: (A) low-dose carboplatin (first-stage experiment) and (B) high-dose carboplatin (second-stage experiment) [59].

doi:10.6342/NTU201704398

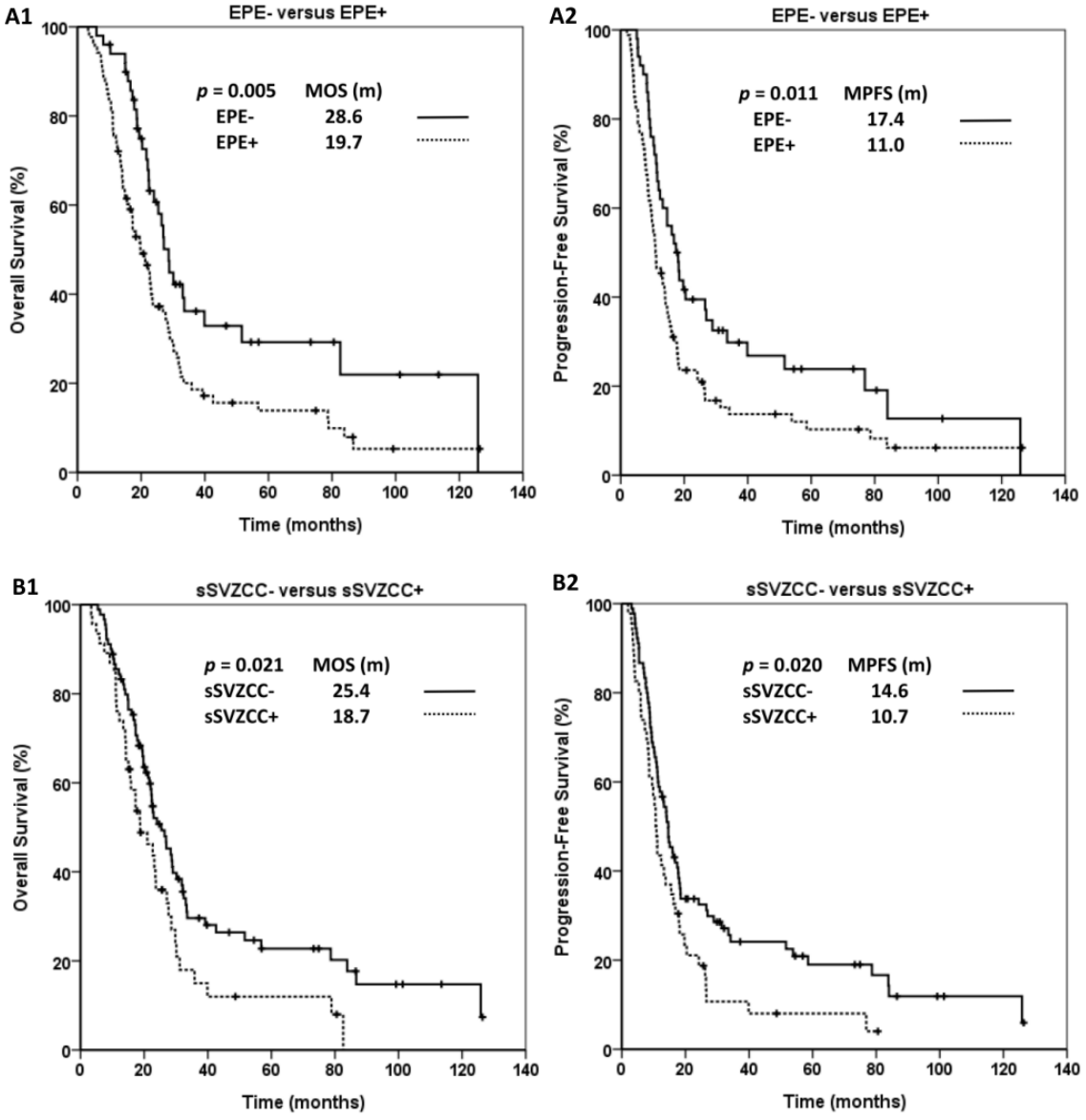

Figure 9. **Kaplan-Meier's estimates** of (A1) OS and (A2) PFS for patients with and without EPE, (B1) OS and (B2) PFS for patients with and without sSVZCC invasion [64].

doi:10.6342/NTU201704398

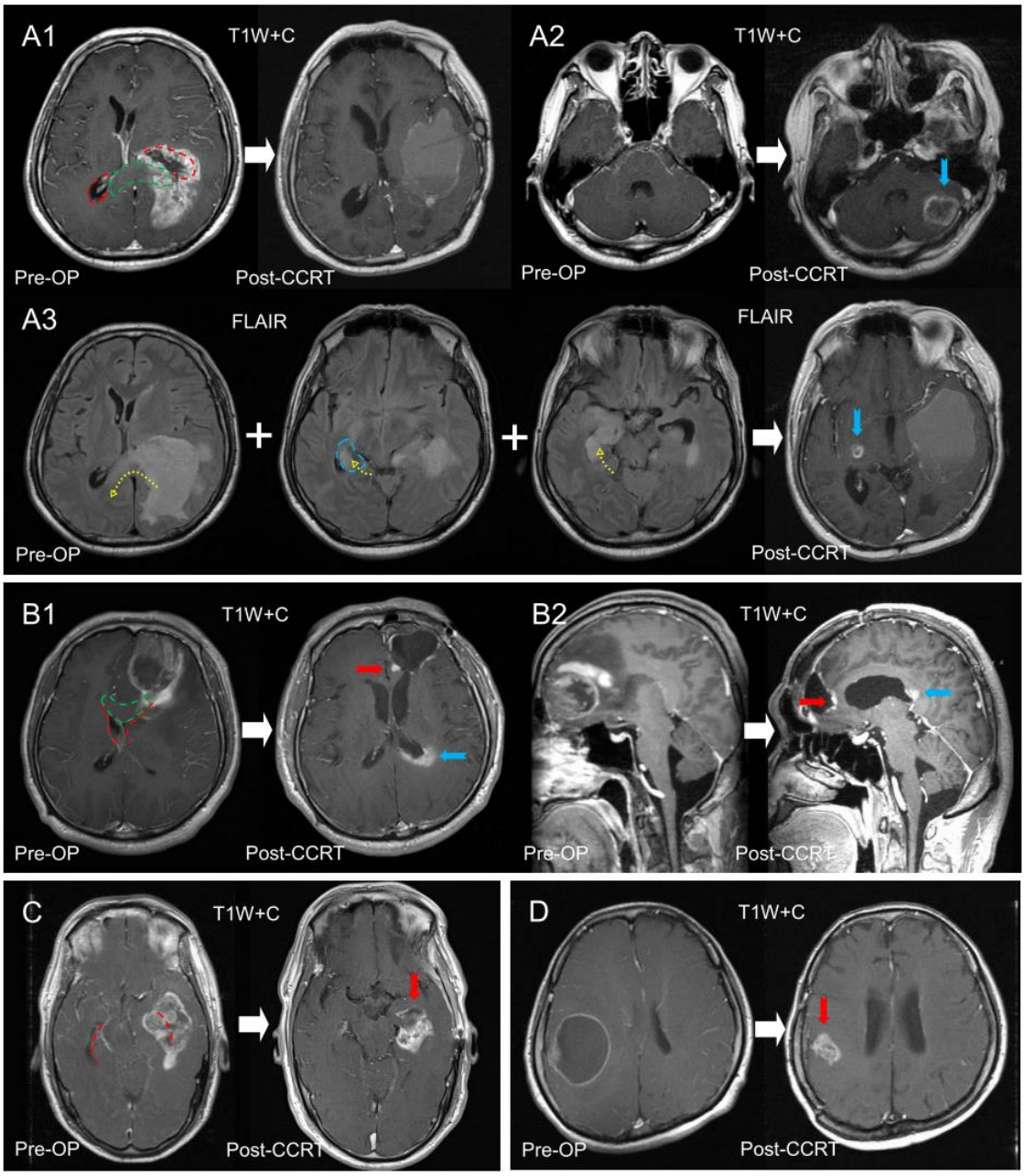

Figure 10. **MRI demonstration of patients with different tumor locations**. Distinct progression patterns after CCRT in 4 patients categorized according to the different combinations of the SVZ and CC invasion. (A1, A2) The patient with synchronous left occipital horn of the SVZ (red dashed lines) and left posterior CC (green dashed lines) invasion exhibited distant progression to the left cerebellum (blue arrow). (A3) Other

doi:10.6342/NTU201704398

progression (blue arrow) developed in the preoperative edematous areas (blue dashed lines), which migrated across the posterior CC to the contralateral hemisphere (yellow dashed arrows). (B1, B2) The patient with synchronous left frontal horn of the SVZ (red dashed lines) and left anterior CC (green dashed lines) invasion showed progression in the tumor bed of the left anterior CC (red arrows) and the distant area at the left posterior CC along the occipital horn (blue arrows). (C) The patient with left temporal horn of the SVZ (red dashed lines) but without CC invasion exhibited progression involving the tumor bed only (red arrow). (D) The patient with neither SVZ nor CC invasion showed progression involving the tumor bed only (red arrow) [23].

doi:10.6342/NTU201704398

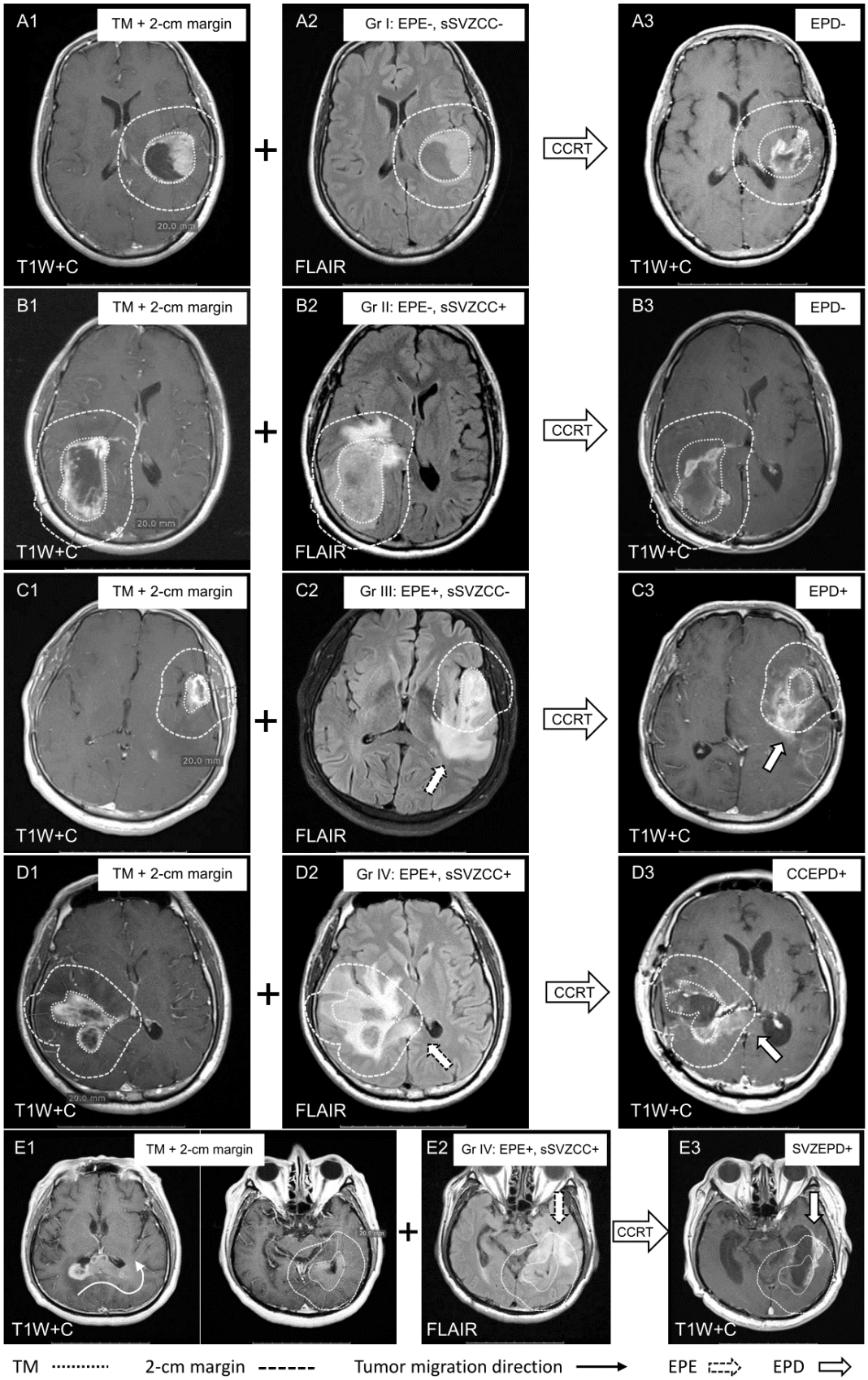

doi:10.6342/NTU201704398

Figure 11. **MRI demonstration of patients with different edema extents and tumor locations**. Distinct progression patterns after CCRT in five patients categorized according to the different combinations of EPE and sSVZCC invasion. A patient with (A1,2) EPE−/sSVZCC− before surgery presented with (A3) local progression without EPD. Another patient with (B1,2) EPE−/sSVZCC+ before surgery presented with (B3) local progression without EPD. Panels C1,2 demonstrate a patient with EPE+/sSVZCC− before surgery, who presented with (C3) local progression with EPD. Panels D1,2 show a patient with EPE+/sSVZCC+ and CCEPE before surgery, who presented with (D3) local progression with EPD along the CC. Panels E1,2 describe a patient with EPE+/sSVZCC+ and SVZEPE before surgery, who presented with (E3) local progression with EPD along the SVZ [64].

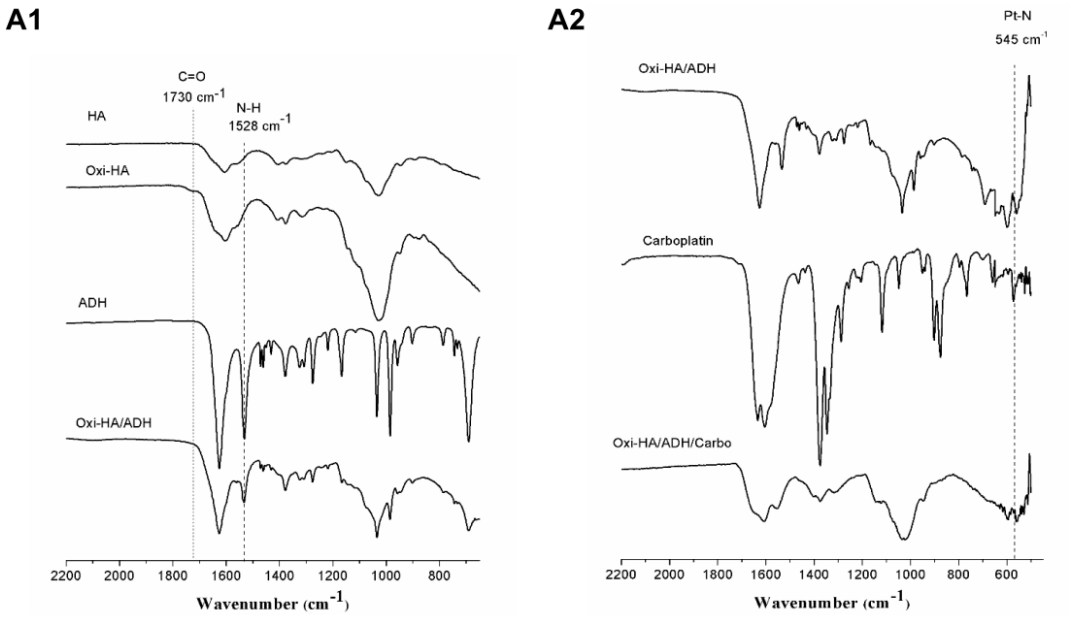

Figure 12. **Illustrations of by FTIR analysis**: (A1) the spectrum peak at 1730 cm-1 of oxi-HA disappeared after mixing oxi-HA with ADH and the appearance of a new forming peak at 1528 cm-1 of oxi-HA/ADH and (A2) the appearance of a new forming peak at 545 cm-1 of oxi-HA/ADH hydrogel carboplatin [59].

doi:10.6342/NTU201704398

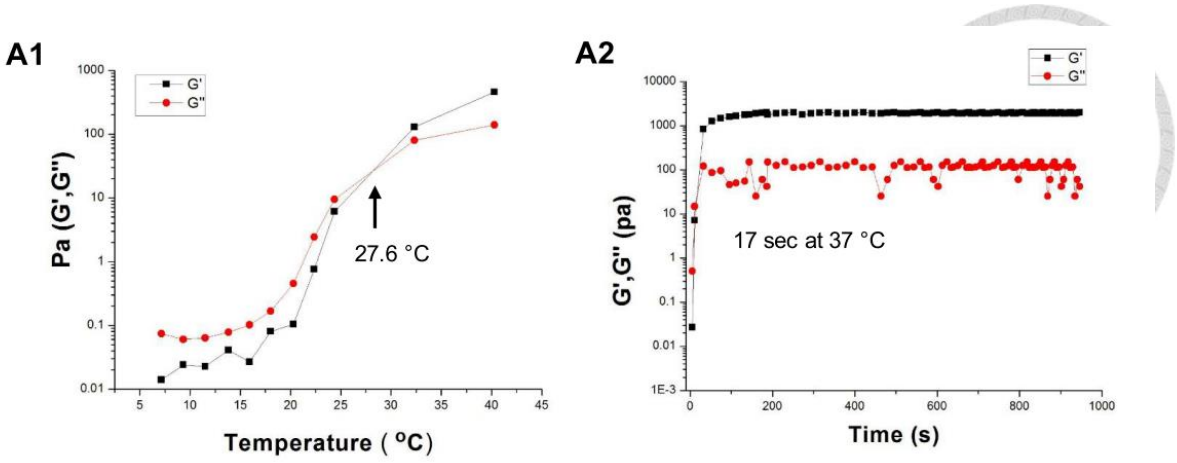

Figure 13. **The rheological properties of oxi-HA/ADH**: (A1) the gelation of oxi-HA/ADH started at temperature higher than 27.6 °C and (A2) the gelling time of oxi-HA/ADH from liquid state to gel state were 17 seconds at 37 °C (body temperature) [59].

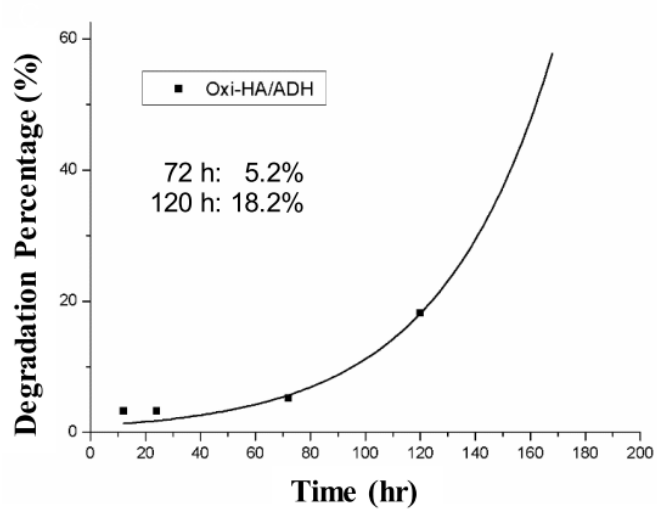

Figure 14. **Degradation properties of oxi-HA/ADH hydrogel**: At 72 and 120 h, degradation percentages for oxi-HA/ADH (Figure 4C) were 5.2% and 18.2%, respectively [59].

doi:10.6342/NTU201704398

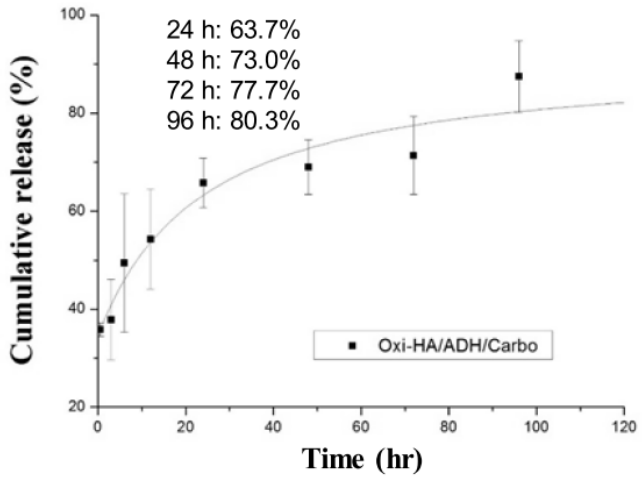

Figure 15. **Drug release profile**: The ICP-MS result demonstrates two phases of the carboplatin release from hydrogel, including a burst release of 63.7% during the first 24 h, followed by a steady release of 16.6% over the 24 to 96 h [59].

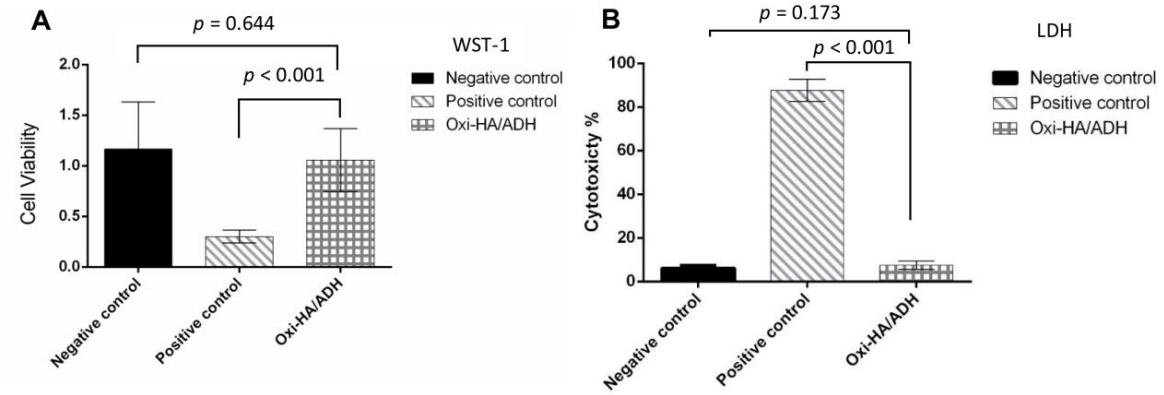

Figure 16. **Biocompatibility of oxi-HA/ADH**: (A) The WST-1 analysis demonstrated the cell viability of 3T3 cells cultured in oxi-HA/ADH hydrogel extraction medium was not significantly different compared with those in the control and negative control groups (p = 0.644). (B) The LDH assay indicated the cytotoxicity oxi-HA/ADH is not significantly different from the negative control group (p = 0.173) [59].

doi:10.6342/NTU201704398

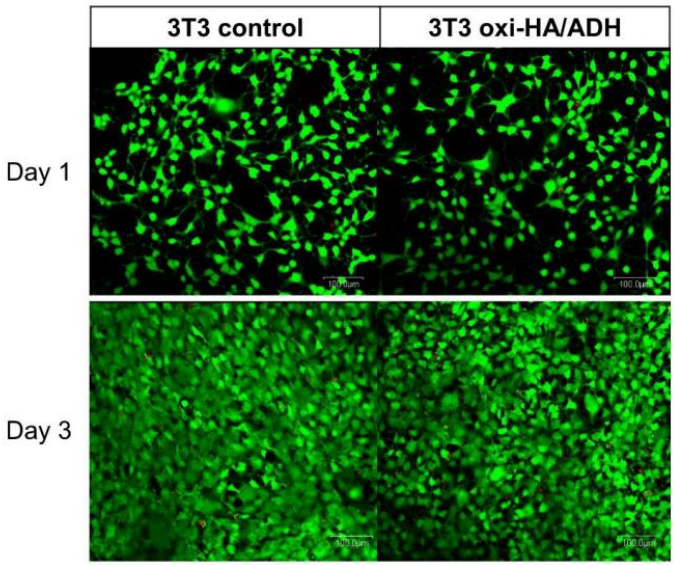

Figure 17. **The LIVE/DEAD staining**: Nearly all the 3T3 cells were viable in the oxi-HA/ADH hydrogel after 3 days' cultivation [59].

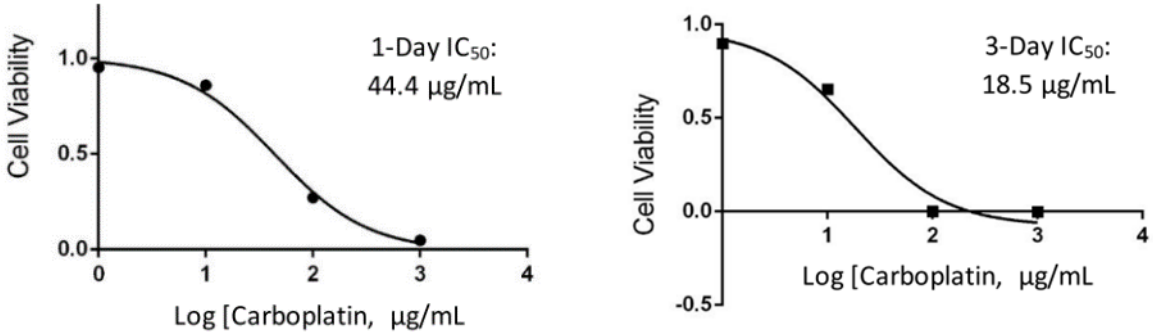

Figure 18. **The IC_{50} test of carboplatin**: The in vitro concentrations of carboplatin to inhibit 50% ALCS1C1 cells to proliferation was 44.4 and 18.5 μg/mL after 1-day and 3-day treatment, respectively [59].

doi:10.6342/NTU201704398

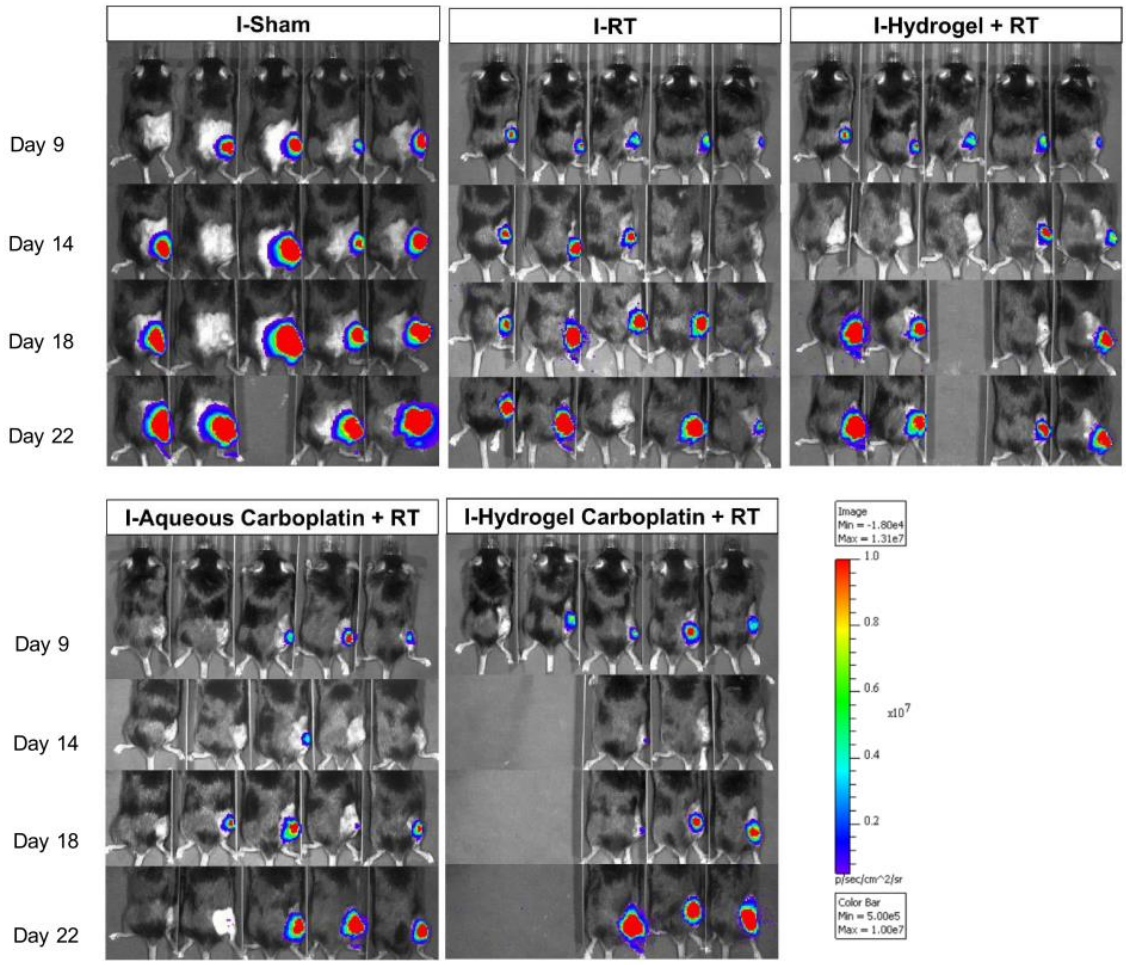

Figure 19. **The BLIs evolution of the first-stage in vivo experiment**. Comparing with the sham group, the BLIs demonstrate the relatively delayed tumor progression in all treatment groups [59].

doi:10.6342/NTU201704398

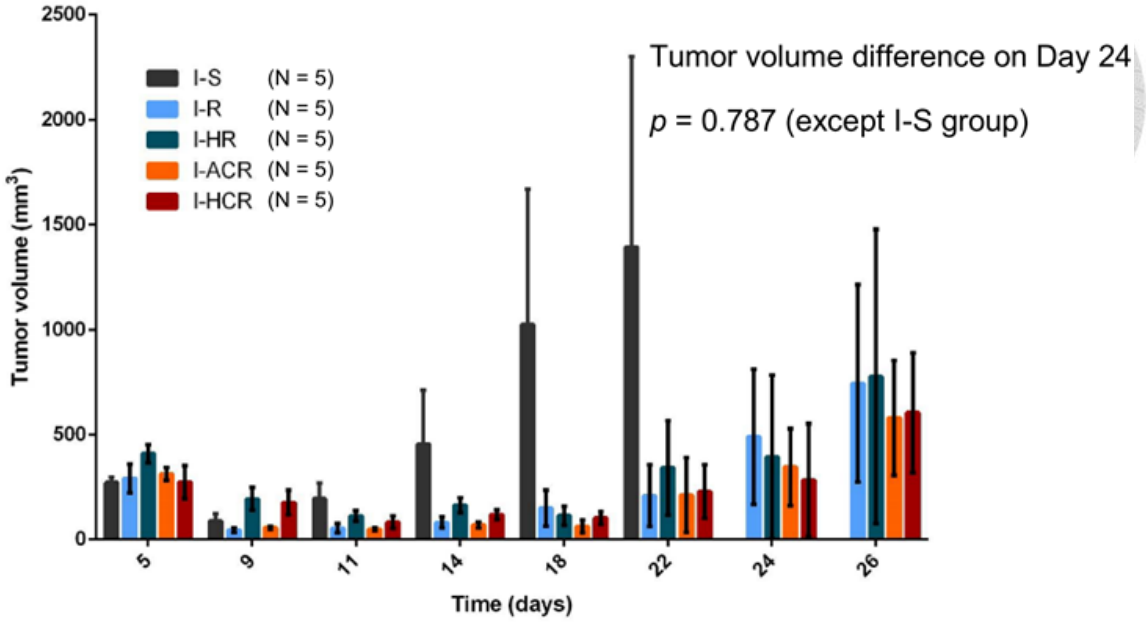

Figure 20. **The tumor volume evolution of the first-stage in vivo experiment**. On day 24, the tumor volume analysis (excepting sham group) by one-way ANOVA showed no difference of tumor progression for RT with and without low-dose carboplatin (p = 0.787) [59].

doi:10.6342/NTU201704398

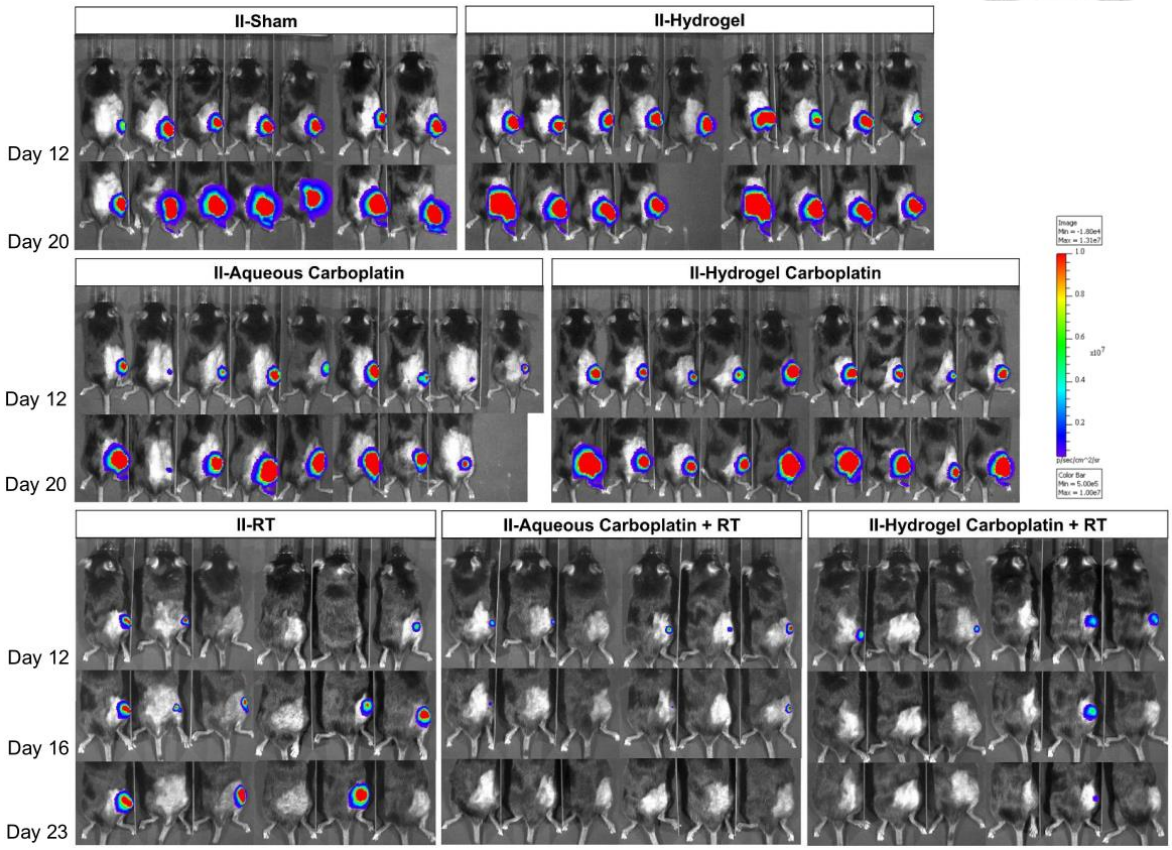

Figure 21. **The BLIs evolution of the second-stage in vivo experiment**. The BLIs demonstrate the tumor nearly complete response in HCR and ACR groups, while tumor progression in other treatment groups [59].

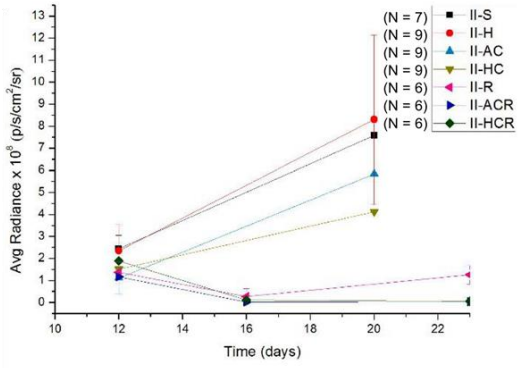

Figure 22. **The bioluminescence signal of the second-stage in vivo experiment** [59].

doi:10.6342/NTU201704398

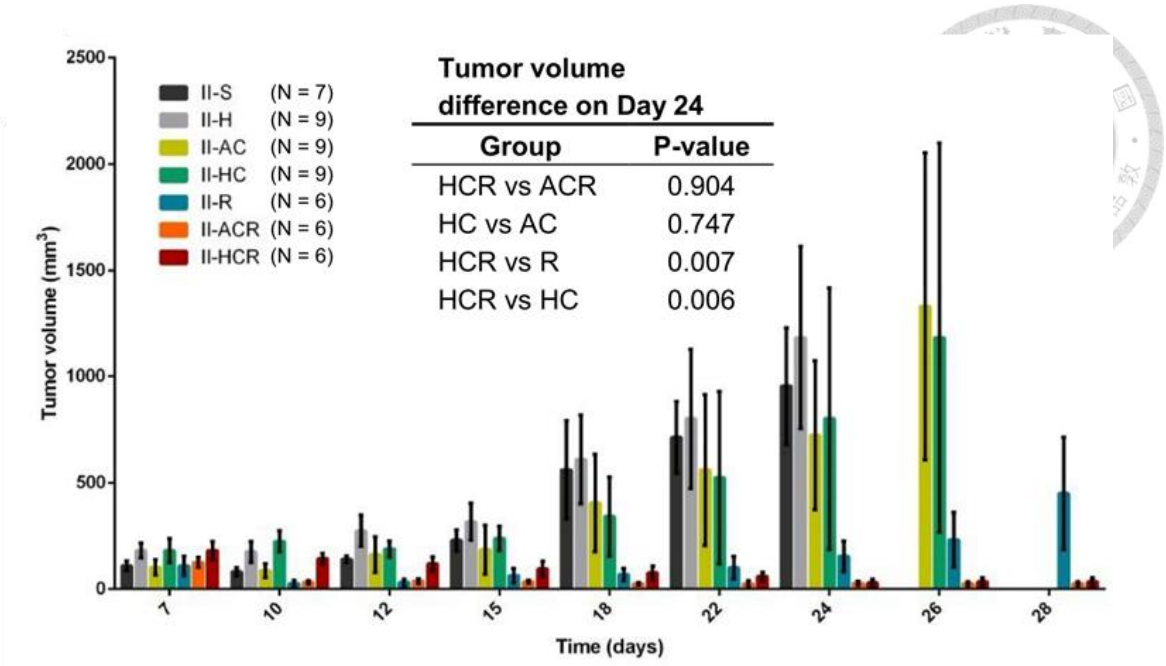

Figure 23. **The tumor volume evolution of the second-stage in vivo experiment**. In ACR and HCR groups, the tumor volume curves demonstrate good tumor control without difference (p = 0.904) [59].

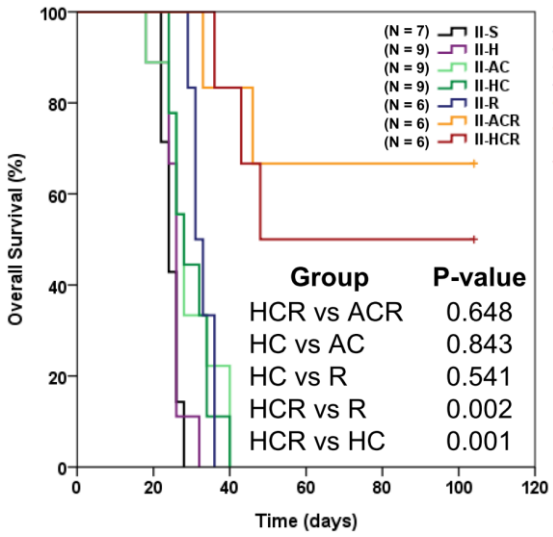

Figure 24. **The survival curves of the second-stage in vivo experiment**: The HCR and ACR groups had 104-day survival rates of 50% and 66.7% without significant difference (p = 0.648) [59].

doi:10.6342/NTU201704398

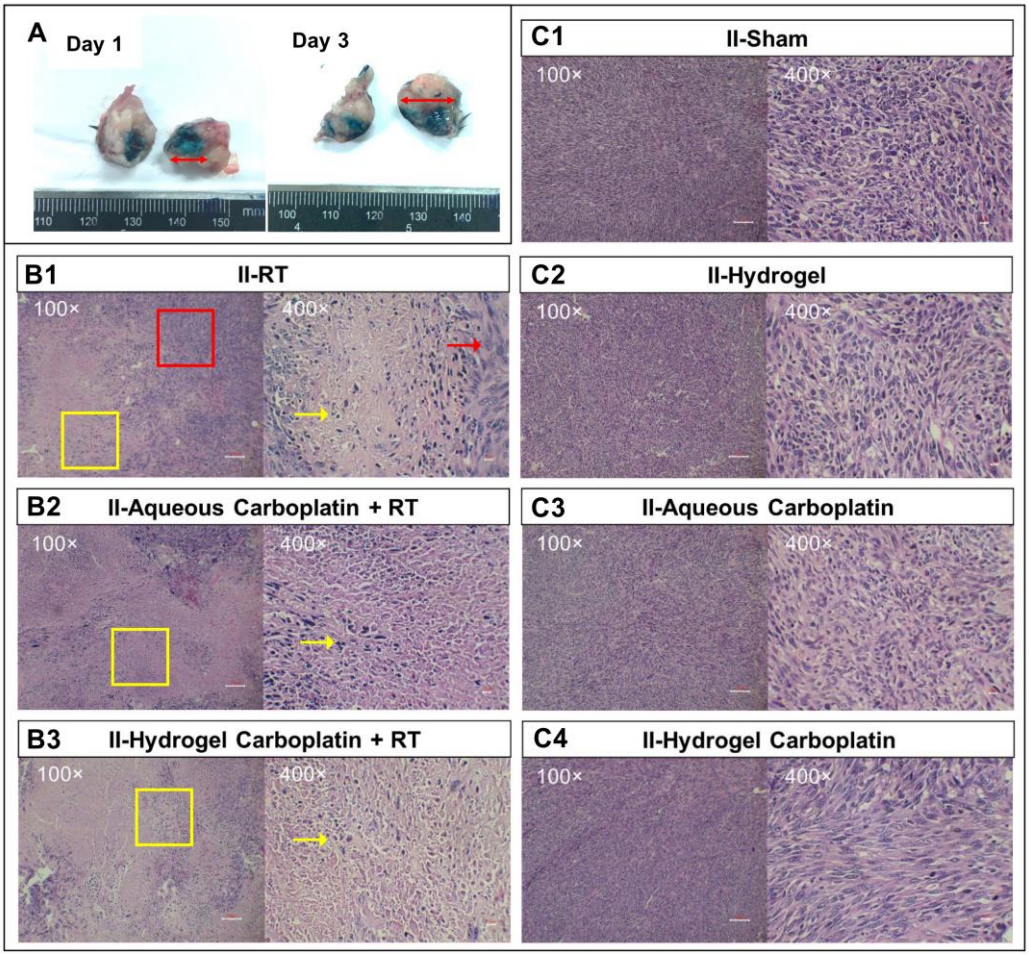

Figure 25. **The gross and histopathological findings of the second-stage in vivo experiment**: (A) The blue area illustrated the diameters of dye distribution 1 day and 3 days after oxi-HA/ADH hydrogel dye injection were 7 and 9 mm, respectively. (B1) The H&E stain of tumor receiving RT showed both cell death (yellow rectangular area at 100× and yellow arrow at 400×) and tumor cell proliferation (red rectangular area at 100× and red arrow at 400×). The H&E stain of tumor receiving either aqueous carboplatin with RT (B2) or hydrogel carboplatin with RT (B3) showed prominent cell death. Contrastingly, H&E stain of tumor cell growth under no treatment (C1) and injection of hydrogel (C2), aqueous carboplatin (C3), and hydrogel carboplatin (C4) all showed tumor cell proliferation only [59].

doi:10.6342/NTU201704398

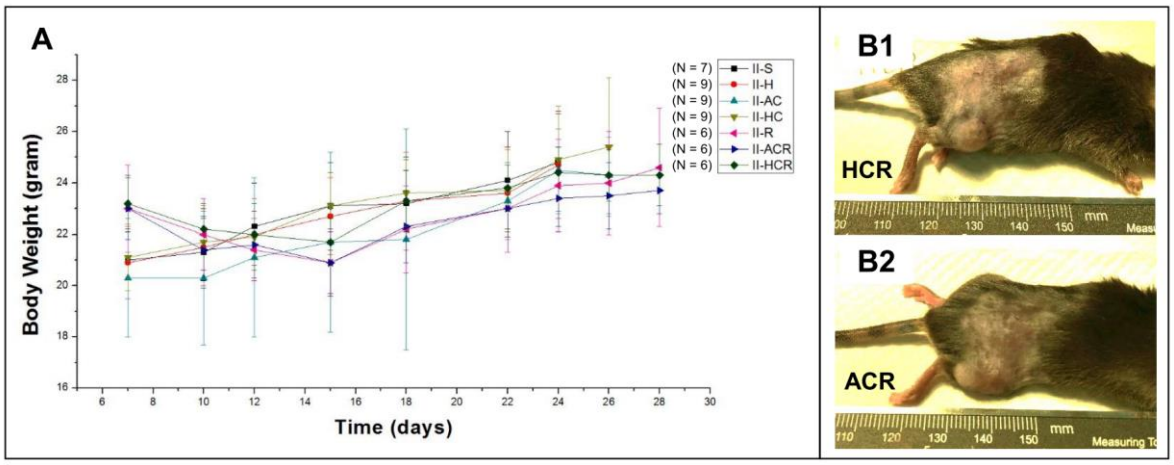

Figure 26. **The weight change and skin reaction of mice in the second-stage in vivo experiment**: (A) Mice weight change in the second-stage experiment. (B) No skin ulcer after treatment of RT with high-dose (C1) hydrogel carboplatin or (C2) aqueous carboplatin [59].

doi:10.6342/NTU201704398

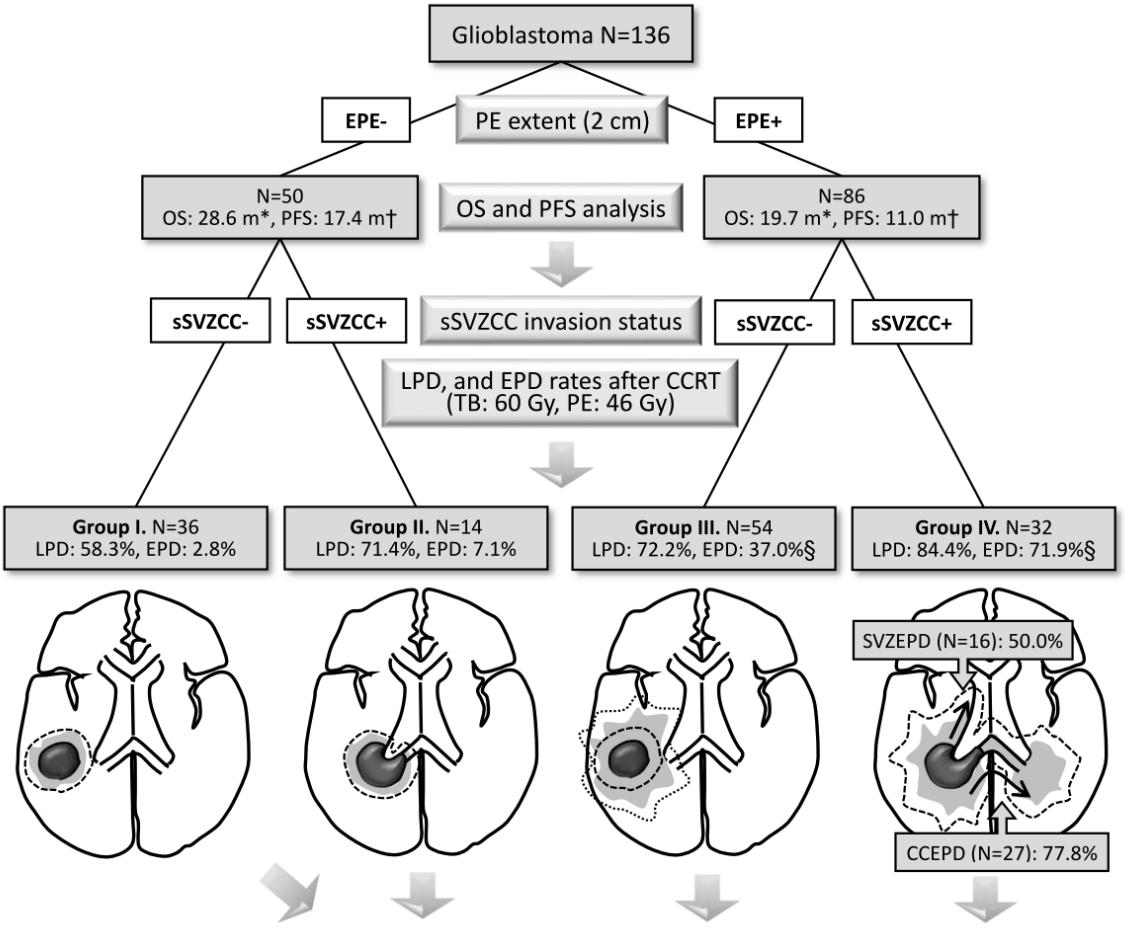

Group	I, II	III	IV
Target delineation	**EORTC guidelines**	**RTOG guidelines**	**Comprehensive delineation**
Targets		***Dose (Gy)/fractions***	
Tumor bed	≥60/30 -----	≥60/30 -----	≥60/30 -----
Preoperative edema	Not applicable	≥46/23 ·····	≥60/30 -----
Potential RT strategy	Hypofractionation	Dose escalation by SIB	Dose escalation
Potential drug administration	TMZ and BCNU wafer	TMZ	TMZ and bevacizumab

*,†,§Statistically significant

Figure 27. **The proposed personalized glioblastoma treatment strategies** [59].

doi:10.6342/NTU201704398

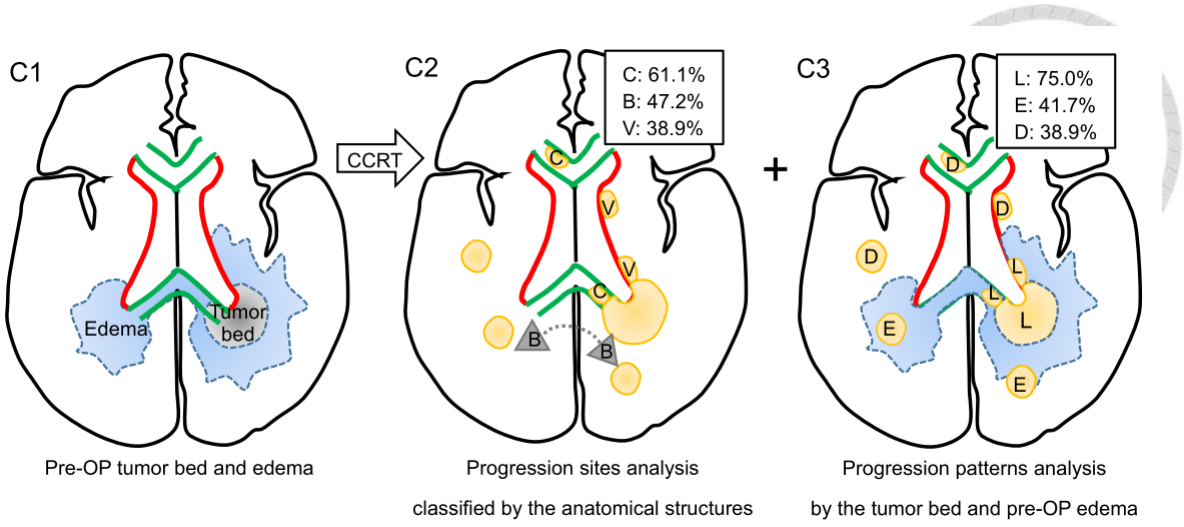

Figure 28. **Progression patterns and sSVZCC invasion**. The comprehensive progression conditions for sSVZCC invasion patients (C1) after CCRT. (C2) The progression sites analysis classified by the anatomical structures. (C3) The progression patterns analysis based on the progressive tumor locations corresponding to the tumor bed and preoperative edematous areas. **Abbreviations**: C, corpus callosum; D, distant; E, edema; H, bilateral hemispheres; L, local; V, ventricles [23]

doi:10.6342/NTU201704398

TABLES

Table 1. Patient characteristics, imaging findings, and treatment modalities stratified by EPE status

Characteristics	Item	Total (N = 136)	EPE− (N = 50)	EPE+ (N = 86)	P-value
		N (%)	N (%)	N (%)	
Sex	Female	58 (42.6)	24 (48.0)	34 (39.5)	0.372
	Male	78 (57.4)	26 (52.0)	52 (60.5)	
Age	20–49	51 (37.5)	18 (36.0)	33 (38.4)	0.855
	50–80	85 (62.5)	32 (64.0)	53 (61.6)	
KPS	80–100	112 (82.4)	40 (80.0)	72 (83.7)	0.644
	40–70	24 (17.6)	10 (20.0)	14 (16.3)	
Tumor Dmax	< 5 cm	60 (44.1)	26 (51.1)	34 (40.4)	0.210
	≥ 5 cm	76 (55.9)	24 (48.0)	52 (60.5)	
sSVZCC invasion	No	90 (66.2)	36 (72.0)	54 (62.8)	0.348
	Yes	46 (33.8)	14 (28.0)	32 (37.2)	
Multiple tumors	No	126 (92.6)	47 (94.0)	79 (91.9)	0.745
	Yes	10 (7.4)	3 (6.0)	7 (8.1)	
IDH-1 mutation*	No	23 (95.8)	10 (90.9)	13 (100)	0.458
	Yes	1 (4.2)	1 (9.1)	0 (0)	
Gross total resection	No	90 (66.2)	33 (66.0)	57 (66.3)	1.000
	Yes	46 (33.8)	17 (34.0)	29 (33.7)	
RT dose (Gy)	≥60	127 (93.4)	47 (94.0)	80 (93.0)	1.000
	54–59	9 (6.6)	3 (6.0)	6 (7.0)	

Abbreviations: Dmax, maximum diameter; EPE, extensive preoperative edema; IDH1, isocitrate dehydrogenase 1; KPS, Karnofsky performance status; N, number; RT, radiotherapy; sSVZCC, synchronous subventricular zone and corpus callosum

*Data available for 24 patients.

doi:10.6342/NTU201704398

Table 2. Univariate analysis results for OS and PFS (N = 136)

Factors		E/N	OS (m)	P-value	E/N	PFS (m)	P-value
Age ≥ 50	No	35/51	23.7	0.323	41/51	14.1	0.368
	Yes	68/85	22.5		74/85	12.6	
KPS ≤ 70	No	84/112	22.9	0.497	94/112	13.2	0.333
	Yes	19/24	22.5		21/24	10.7	
Tumor Dmax ≥ 5 cm	No	45/60	22.2	0.338	52/60	13.1	0.225
	Yes	58/76	23.2		63/76	13.9	
EPE (≥ 2 cm)	No	31/50	28.6	0.005*	39/50	17.4	0.011*
	Yes	72/86	19.7		76/86	11.0	
sSVZCC invasion	No	65/90	25.4	0.021*	73/90	14.6	0.020*
	Yes	38/46	18.7		42/46	10.7	
Gross total resection	No	70/90	22.1	0.088	78/90	11.4	0.116
	Yes	33/46	26.9		37/46	14.6	

Abbreviations: Dmax, maximum diameter; E, event; EPE, extensive preoperative edema; KPS, Karnofsky performance status; N, number; OS, overall survival; PFS, progression-free survival; sSVZCC, synchronous subventricular zone and corpus callosum

*Statistically significant

Table 3. Multivariate Cox proportional hazards results for shorter OS and PFS combined with different various anatomical factors (N = 136)

	OS			PFS		
Factors	**HR**	**95% CI**	***P*-value**	**HR**	**95% CI**	***P*-value**
Age ≥ 50	1.36	0.89–2.07	0.156	1.29	0.86–1.94	0.221
KPS ≤ 70	0.99	0.58–1.71	0.978	1.06	0.63–1.78	0.825
Tumor Dmax ≥ 5 cm	0.79	0.51–1.23	0.300	0.71	0.47–1.07	0.104
EPE (≥ 2 cm)	1.98	1.28–3.05	0.002*	1.84	1.23–2.76	0.003*
sSVZCC invasion	1.50	0.96–2.34	0.076	1.56	1.03–2.38	0.038*
Gross total resection	0.76	0.48–1.21	0.245	0.83	0.54–1.28	0.394

Abbreviations: CI, confidence interval; Dmax, maximum diameter; EPE, extensive preoperative edema; HR, hazard ratio; KPS, Karnofsky performance status; N, number; OS, overall survival; PFS, progression-free survival; sSVZCC, synchronous subventricular zone and corpus callosum

*Statistically significant

doi:10.6342/NTU201704398

Table 4. Univariate analysis results for OS and PFS stratified by sSVZCC invasion status the in the EPE− and EPE+ groups

Factors	sSVZCC invasion	E/N	OS (m)	P-value	E/N	PFS (m)	P-value
EPE−	No	21/36	28.6	0.148	27/36	18.1	0.249
(N = 50)	Yes	10/14	27.1		12/14	12.4	
EPE+	No	44/54	21.3	0.106	46/54	12.6	0.092
(N = 86)	Yes	28/32	15.6		30/32	9.9	

Abbreviations: CI, confidence interval; Dmax, maximum diameter; E, event; EPE, extensive preoperative edema; HR, hazard ratio; KPS, Karnofsky performance status; N, number; OS, overall survival; PFS, progression-free survival; sSVZCC, synchronous subventricular zone and corpus callosum

doi:10.6342/NTU201704398

Table 5. Progression patterns and sites stratified by EPE and sSVZCC invasion (N = 136)

EPE− patients (N = 50)		sSVZCC invasion, N (%)		P-value
Progression patterns		No (N=36), Gr I	Yes (N=14), Gr II	
EPD	No	35 (97.2)	13 (92.9)	0.486
	Yes	1 (2.8)	1 (7.1)	
Local (tumor bed)	No	15 (41.7)	4 (28.6)	0.522
	Yes	21 (58.3)	10 (71.4)	
Regional (discrete)	No	35 (97.2)	14 (100)	1.000
	Yes	1 (2.8)	0 (0)	
Distant	No	30 (83.3)	11 (78.6)	0.697
	Yes	6 (16.7)	3 (21.4)	
EPE+ patients (N = 86)		**sSVZCC invasion, N (%)**		**P-value**
Progression patterns		No (N=54), Gr III	Yes (N=32), Gr IV	
EPD	No	34 (63.0)	9 (28.1)	0.003*
	Yes	20 (37.0)	23 (71.9)	
Local (tumor bed)	No	15 (27.8)	5 (15.6)	0.291
	Yes	39 (72.2)	27 (84.4)	
Regional (discrete)	No	46 (85.2)	14 (43.8)	<0.001*
	Yes	8 (14.8)	18 (56.3)	
Distant	No	42 (77.8)	21 (65.6)	0.313
	Yes	12 (22.2)	11 (34.4)	
EPE+, sSVZCC+ (N = 32)		**CCEPE**		**P-value**
Progression patterns		No (N=5)	Yes (N=27)	
CCEPD	No	4 (80.0)	6 (22.2)	0.024*
	Yes	1 (20.0)	21 (77.8)	
EPE+, sSVZCC+ (N = 32)		**SVZEPE**		**P-value**
Progression patterns		No (N=16)	Yes (N=16)	
SVZEPD	No	15 (93.8)	8 (50.0)	0.015*
	Yes	1 (6.3)	8 (50.0)	

Abbreviations: CCEPD, extensive progressive disease along the corpus callosum; CCEPE, extensive preoperative edema along the corpus callosum; EPD, extensive progressive disease; EPE, extensive preoperative edema; Gr, group; N, patient number; sSVZCC, synchronous subventricular zone and corpus callosum; SVZEPD, extensive progressive disease along the subventricular zone; SVZEPE, extensive preoperative edema along the subventricular zone

*Statistically significant (Fisher's exact test)

doi:10.6342/NTU201704398

Table 6. Progression patterns and sites stratified by RT techniques

All patients (N = 136)		RT techniques, N (%)		P-value
Progression patterns		3DCRT (N = 21)	IMRT* (N = 115)	
EPD	No	17 (81.0)	74 (64.4)	0.207
	Yes	4 (19.0)	41 (35.7)	
Local (tumor bed)	No	6 (28.6)	33 (28.7)	1.000
	Yes	15 (71.4)	82 (71.3)	
Regional (discrete)	No	19 (90.5)	90 (78.3)	0.247
	Yes	2 (9.5)	25 (21.7)	
Distant	No	16 (76.2)	88 (76.5)	1.000
	Yes	5 (23.8)	27 (23.5)	

Abbreviations: 3DCRT, 3-dimensional conformal radiation therapy; EPD, extensive progressive disease; IMRT, intensity-modulated radiation therapy; RT, radiotherapy

*IMRT or more advanced techniques including volumetric-modulated arc therapy, and tomotherapy

Table 7. Analysis of survival in the first-stage in vivo experiment

Treatment group		Median OS (day)	P-Value
I-S	(N = 5)	21	R vs HR vs HCR vs ACR: 0.53
I-R	(N = 5)	35	
I-HR	(N = 5)	35	
I-HCR	(N = 5)	35	
I-ACR	(N = 5)	35	

Abbreviations: ACR, radiotherapy with aqueous carboplatin; HCR, radiotherapy with hydrogel carboplatin; HR, radiotherapy with hydrogel; OS, overall survival; R, radiotherapy; S, sham.

doi:10.6342/NTU201704398

Table 8. Analysis of survival in the second-stage in vivo experiment

Treatment group		Median OS (day)	104-day survival (%)	P-Value
II-S	(N = 7)	24	0	HCR vs ACR: 0.648
II-H	(N = 9)	26	0	HC vs AC: 0.843
II-AC	(N = 9)	28	0	HCR vs R: 0.002*
II-HC	(N = 9)	28	0	HCR vs HC: 0.001*
II-R	(N = 6)	31	0	R vs HC: 0.541
II-ACR	(N = 6)	Not reached	67	
II-HCR	(N = 6)	48	50	

Abbreviations: AC, aqueous carboplatin; ACR, radiotherapy with aqueous carboplatin; H, hydrogel; HC, hydrogel carboplatin; HCR, radiotherapy with hydrogel carboplatin; HR, radiotherapy with hydrogel; OS, overall survival; R, radiotherapy; S, sham.

Table 9. Analysis of blood samples in the second-stage in vivo experiment

CBC/BCS	Unit	Reference	II-S (N = 3)	II-H (N = 3)	II-AC (N = 3)	II-HC (N = 3)
Hb	g/dL	11.1–16.4	11.9 ± 0.8	13.1 ± 0.5	11.3 ± 1	12.7 ± 0.7
PLT	K/μL	385–890	492 ± 374	889 ± 9	666 ± 167	555 ± 326
WBC	K/μL	1.8–5.2	5.71 ± 2	2.89 ± 2	3.13 ± 0.7	3.51 ± 2
ALT	U/L	28–129	39 ± 13	56 ± 32	43 ± 4	68 ± 15
AST	U/L	46–392	252 ± 268	114 ± 61	159 ± 68	221 ± 77
BUN	mg/dL	7–28	26 ± 4	21 ± 2	25 ± 4	23 ± 2
Cre	mg/dL	0.2–0.5	0.2	0.2	0.2	0.2

Abbreviations: ALT, alanine aminotransferase; AST, aspartate aminotransferase; BCS, biochemistry study; BUN, blood urea nitrogen; CBC, complete blood count; Cre, creatinine; Hb, hemoglobin; PLT, platelet; WBC, white blood cell.

doi:10.6342/NTU201704398

REFERENCES

[1] Q.T. Ostrom, L. Bauchet, F.G. Davis, I. Deltour, J.L. Fisher, C.E. Langer, M. Pekmezci, J.A. Schwartzbaum, M.C. Turner, K.M. Walsh, M.R. Wrensch, J.S. Barnholtz-Sloan, The epidemiology of glioma in adults: a "state of the science" review, Neuro Oncol 16(7) (2014) 896-913.

[2] Cancer Registry Annual Report 2014, Health Promotion Administration, Ministry of Health and Welfare, Taiwan, 2016, p. 93.

[3] Cancer Registry Annual Report 2013, Health Promotion Administration, Ministry of Health and Welfare, Taiwan, 2015, p. 93.

[4] Cancer Registry Annual Report 2012, Health Promotion Administration, Ministry of Health and Welfare, Taiwan, 2014, p. 93.

[5] P.Y. Wen, S. Kesari, Malignant gliomas in adults, N Engl J Med 359(5) (2008) 492-507.

[6] S. Cha, Update on brain tumor imaging: from anatomy to physiology, AJNR Am J Neuroradiol 27(3) (2006) 475-87.

[7] J. Li, M. Wang, M. Won, E.G. Shaw, C. Coughlin, W.J. Curran, Jr., M.P. Mehta, Validation and simplification of the Radiation Therapy Oncology Group recursive partitioning analysis classification for glioblastoma, International journal of radiation oncology, biology, physics 81(3) (2011) 623-30.

[8] R.O. Mirimanoff, T. Gorlia, W. Mason, M.J. Van den Bent, R.D. Kortmann, B. Fisher, M. Reni, A.A. Brandes, J. Curschmann, S. Villa, G. Cairncross, A. Allgeier, D. Lacombe, R. Stupp, Radiotherapy and temozolomide for newly diagnosed glioblastoma: recursive partitioning analysis of the EORTC 26981/22981-NCIC CE3 phase III randomized trial,

doi:10.6342/NTU201704398

Journal of clinical oncology : official journal of the American Society of Clinical Oncology 24(16) (2006) 2563-9.

[9] H.K. Liang, C.W. Wang, H.M. Tseng, C.Y. Huang, K.H. Lan, Y.H. Chen, S.L. You, J.C. Cheng, A.L. Cheng, S.H. Kuo, Preoperative prognostic neurologic index for glioblastoma patients receiving tumor resection, Annals of surgical oncology 21(12) (2014) 3992-8.

[10] M.E. Hegi, A.C. Diserens, T. Gorlia, M.F. Hamou, N. de Tribolet, M. Weller, J.M. Kros, J.A. Hainfellner, W. Mason, L. Mariani, J.E. Bromberg, P. Hau, R.O. Mirimanoff, J.G. Cairncross, R.C. Janzer, R. Stupp, MGMT gene silencing and benefit from temozolomide in glioblastoma, The New England journal of medicine 352(10) (2005) 997-1003.

[11] S.E. Combs, S. Rieken, W. Wick, A. Abdollahi, A. von Deimling, J. Debus, C. Hartmann, Prognostic significance of IDH-1 and MGMT in patients with glioblastoma: one step forward, and one step back?, Radiat Oncol 6 (2011) 115.

[12] M.D. Walker, S.B. Green, D.P. Byar, E. Alexander, Jr., U. Batzdorf, W.H. Brooks, W.E. Hunt, C.S. MacCarty, M.S. Mahaley, Jr., J. Mealey, Jr., G. Owens, J. Ransohoff, 2nd, J.T. Robertson, W.R. Shapiro, K.R. Smith, Jr., C.B. Wilson, T.A. Strike, Randomized comparisons of radiotherapy and nitrosoureas for the treatment of malignant glioma after surgery, N Engl J Med 303(23) (1980) 1323-9.

[13] H. Athanassiou, M. Synodinou, E. Maragoudakis, M. Paraskevaidis, C. Verigos, D. Misailidou, D. Antonadou, G. Saris, K. Beroukas, P. Karageorgis, Randomized phase II study of temozolomide and radiotherapy compared with radiotherapy alone in newly diagnosed glioblastoma multiforme, J Clin Oncol 23(10) (2005) 2372-7.

[14] R. Stupp, P.Y. Dietrich, S. Ostermann Kraljevic, A. Pica, I. Maillard, P. Maeder, R. Meuli, R. Janzer, G. Pizzolato, R. Miralbell, F. Porchet, L. Regli, N. de Tribolet, R.O.

doi:10.6342/NTU201704398

Mirimanoff, S. Leyvraz, Promising survival for patients with newly diagnosed glioblastoma multiforme treated with concomitant radiation plus temozolomide followed by adjuvant temozolomide, J Clin Oncol 20(5) (2002) 1375-82.

[15] R. Stupp, W.P. Mason, M.J. van den Bent, M. Weller, B. Fisher, M.J. Taphoorn, K. Belanger, A.A. Brandes, C. Marosi, U. Bogdahn, J. Curschmann, R.C. Janzer, S.K. Ludwin, T. Gorlia, A. Allgeier, D. Lacombe, J.G. Cairncross, E. Eisenhauer, R.O. Mirimanoff, R. European Organisation for, T. Treatment of Cancer Brain, G. Radiotherapy, G. National Cancer Institute of Canada Clinical Trials, Radiotherapy plus concomitant and adjuvant temozolomide for glioblastoma, The New England journal of medicine 352(10) (2005) 987-96.

[16] A.A. Brandes, A. Tosoni, E. Franceschi, G. Sotti, G. Frezza, P. Amista, L. Morandi, F. Spagnolli, M. Ermani, Recurrence pattern after temozolomide concomitant with and adjuvant to radiotherapy in newly diagnosed patients with glioblastoma: correlation With MGMT promoter methylation status, J Clin Oncol 27(8) (2009) 1275-9.

[17] M.W. McDonald, H.K. Shu, W.J. Curran, Jr., I.R. Crocker, Pattern of failure after limited margin radiotherapy and temozolomide for glioblastoma, Int J Radiat Oncol Biol Phys 79(1) (2011) 130-6.

[18] B.J. Gebhardt, M.C. Dobelbower, W.H. Ennis, A.K. Bag, J.M. Markert, J.B. Fiveash, Patterns of failure for glioblastoma multiforme following limited-margin radiation and concurrent temozolomide, Radiat Oncol 9 (2014) 130.

[19] A. Lattermann, M. Baumann, M. Krause, Clinical trials for personalized glioblastoma radiotherapy: Markers for efficacy and late toxicity but often delayed treatment - Does that matter?, Radiother Oncol 118(1) (2016) 211-3.

doi:10.6342/NTU201704398

[20] M. Niyazi, M. Brada, A.J. Chalmers, S.E. Combs, S.C. Erridge, A. Fiorentino, A.L. Grosu, F.J. Lagerwaard, G. Minniti, R.O. Mirimanoff, U. Ricardi, S.C. Short, D.C. Weber, C. Belka, ESTRO-ACROP guideline "target delineation of glioblastomas", Radiother Oncol 118(1) (2016) 35-42.

[21] E.P. Jansen, L.G. Dewit, M. van Herk, H. Bartelink, Target volumes in radiotherapy for high-grade malignant glioma of the brain, Radiother Oncol 56(2) (2000) 151-6.

[22] L. Chen, K.L. Chaichana, L. Kleinberg, X. Ye, A. Quinones-Hinojosa, K. Redmond, Glioblastoma recurrence patterns near neural stem cell regions, Radiother Oncol 116(2) (2015) 294-300.

[23] T.H. Liang, S.H. Kuo, C.W. Wang, W.Y. Chen, C.Y. Hsu, S.F. Lai, H.M. Tseng, S.L. You, C.M. Chen, W.Y. Tseng, Adverse prognosis and distinct progression patterns after concurrent chemoradiotherapy for glioblastoma with synchronous subventricular zone and corpus callosum invasion, Radiother Oncol 118(1) (2016) 16-23.

[24] S. Adeberg, L. Konig, T. Bostel, S. Harrabi, T. Welzel, J. Debus, S.E. Combs, Glioblastoma recurrence patterns after radiation therapy with regard to the subventricular zone, Int J Radiat Oncol Biol Phys 90(4) (2014) 886-93.

[25] N.F. Jafri, J.L. Clarke, V. Weinberg, I.J. Barani, S. Cha, Relationship of glioblastoma multiforme to the subventricular zone is associated with survival, Neuro Oncol 15(1) (2013) 91-6.

[26] S. Adeberg, T. Bostel, L. Konig, T. Welzel, J. Debus, S.E. Combs, A comparison of long-term survivors and short-term survivors with glioblastoma, subventricular zone involvement: a predictive factor for survival?, Radiat Oncol 9 (2014) 95.

doi:10.6342/NTU201704398

[27] A.M. Mistry, A.T. Hale, L.B. Chambless, K.D. Weaver, R.C. Thompson, R.A. Ihrie, Influence of glioblastoma contact with the lateral ventricle on survival: a meta-analysis, J Neurooncol (2016).

[28] D.A. Lim, S. Cha, M.C. Mayo, M.H. Chen, E. Keles, S. VandenBerg, M.S. Berger, Relationship of glioblastoma multiforme to neural stem cell regions predicts invasive and multifocal tumor phenotype, Neuro Oncol 9(4) (2007) 424-9.

[29] K.J. Steltzer, K.I. Sauve, A.M. Spence, T.W. Griffin, M.S. Berger, Corpus callosum involvement as a prognostic factor for patients with high-grade astrocytoma, International journal of radiation oncology, biology, physics 38(1) (1997) 27-30.

[30] K. Dziurzynski, D. Blas-Boria, D. Suki, D.P. Cahill, S.S. Prabhu, V. Puduvalli, N. Levine, Butterfly glioblastomas: a retrospective review and qualitative assessment of outcomes, Journal of neuro-oncology 109(3) (2012) 555-63.

[31] K.L. Chaichana, I. Jusue-Torres, A.M. Lemos, A. Gokaslan, E.E. Cabrera-Aldana, A. Ashary, A. Olivi, A. Quinones-Hinojosa, The butterfly effect on glioblastoma: is volumetric extent of resection more effective than biopsy for these tumors?, Journal of neuro-oncology 120(3) (2014) 625-34.

[32] C.X. Wu, G.S. Lin, Z.X. Lin, J.D. Zhang, S.Y. Liu, C.F. Zhou, Peritumoral edema shown by MRI predicts poor clinical outcome in glioblastoma, World J Surg Oncol 13 (2015) 97.

[33] A.I. Mehta, A. Linninger, M.S. Lesniak, H.H. Engelhard, Current status of intratumoral therapy for glioblastoma, J Neurooncol 125(1) (2015) 1-7.

[34] W.K. Xing, C. Shao, Z.Y. Qi, C. Yang, Z. Wang, The role of Gliadel wafers in the treatment of newly diagnosed GBM: a meta-analysis, Drug Des Devel Ther 9 (2015) 3341-8.

doi:10.6342/NTU201704398

[35] L.S. Ashby, K.A. Smith, B. Stea, Gliadel wafer implantation combined with standard radiotherapy and concurrent followed by adjuvant temozolomide for treatment of newly diagnosed high-grade glioma: a systematic literature review, World J Surg Oncol 14(1) (2016) 225.

[36] A. Quinones-Hinojosa, N. Sanai, M. Soriano-Navarro, O. Gonzalez-Perez, Z. Mirzadeh, S. Gil-Perotin, R. Romero-Rodriguez, M.S. Berger, J.M. Garcia-Verdugo, A. Alvarez-Buylla, Cellular composition and cytoarchitecture of the adult human subventricular zone: a niche of neural stem cells, J Comp Neurol 494(3) (2006) 415-34.

[37] F. Doetsch, A. Alvarez-Buylla, Network of tangential pathways for neuronal migration in adult mammalian brain, Proceedings of the National Academy of Sciences of the United States of America 93(25) (1996) 14895-900.

[38] G. Kempermann, Why new neurons? Possible functions for adult hippocampal neurogenesis, The Journal of neuroscience : the official journal of the Society for Neuroscience 22(3) (2002) 635-8.

[39] J. Kiernan, R. Rajakumar, Barr's the human nervous system: an anatomical viewpoint, Lippincott Williams & Wilkins2013.

[40] H. Wolburg, S. Noell, P. Fallier-Becker, A.F. Mack, K. Wolburg-Buchholz, The disturbed blood-brain barrier in human glioblastoma, Mol Aspects Med 33(5-6) (2012) 579-89.

[41] A.B. Fleming, W.M. Saltzman, Pharmacokinetics of the carmustine implant, Clin Pharmacokinet 41(6) (2002) 403-19.

doi:10.6342/NTU201704398

[42] C. Bastiancich, P. Danhier, V. Preat, F. Danhier, Anticancer drug-loaded hydrogels as drug delivery systems for the local treatment of glioblastoma, J Control Release 243 (2016) 29-42.

[43] D. Fortin, P.A. Morin, F. Belzile, D. Mathieu, F.M. Pare, Intra-arterial carboplatin as a salvage strategy in the treatment of recurrent glioblastoma multiforme, J Neurooncol 119(2) (2014) 397-403.

[44] M. Ronghe, D. Hargrave, U. Bartels, U. Tabori, S. Vaidya, C. Chandler, A. Kulkarni, E. Bouffet, Vincristine and carboplatin chemotherapy for unresectable and/or recurrent low-grade astrocytoma of the brainstem, Pediatr Blood Cancer 55(3) (2010) 471-7.

[45] M. Roskies, E. Kay-Rivest, M.A. Mascarella, K. Sultanem, A. Mlynarek, M. Hier, Survival outcomes in patients with oropharyngeal cancer treated with carboplatin/paclitaxel and concurrent radiotherapy, J Otolaryngol Head Neck Surg 45(1) (2016) 50.

[46] D. Wang, S.J. Lippard, Cellular processing of platinum anticancer drugs, Nat Rev Drug Discov 4(4) (2005) 307-20.

[47] M. Rezaee, D.J. Hunting, L. Sanche, New insights into the mechanism underlying the synergistic action of ionizing radiation with platinum chemotherapeutic drugs: the role of low-energy electrons, Int J Radiat Oncol Biol Phys 87(4) (2013) 847-53.

[48] L. Bobyk, M. Edouard, P. Deman, J. Rousseau, J.F. Adam, J.L. Ravanat, F. Esteve, J. Balosso, R.F. Barth, H. Elleaume, Intracerebral delivery of carboplatin in combination with either 6 MV photons or monoenergetic synchrotron X-rays are equally efficacious for treatment of the F98 rat glioma, J Exp Clin Cancer Res 31 (2012) 78.

doi:10.6342/NTU201704398

[49] M. Shi, D. Fortin, L. Sanche, B. Paquette, Convection-enhancement delivery of platinum-based drugs and Lipoplatin(TM) to optimize the concomitant effect with radiotherapy in F98 glioma rat model, Invest New Drugs 33(3) (2015) 555-63.

[50] W. Yang, T. Huo, R.F. Barth, N. Gupta, M. Weldon, J.C. Grecula, B.D. Ross, B.A. Hoff, T.C. Chou, J. Rousseau, H. Elleaume, Convection enhanced delivery of carboplatin in combination with radiotherapy for the treatment of brain tumors, J Neurooncol 101(3) (2011) 379-90.

[51] W. Yang, R.F. Barth, T. Huo, R.J. Nakkula, M. Weldon, N. Gupta, L. Agius, J.C. Grecula, Radiation therapy combined with intracerebral administration of carboplatin for the treatment of brain tumors, Radiat Oncol 9 (2014) 25.

[52] T. Shahar, Z. Ram, A.A. Kanner, Convection-enhanced delivery catheter placements for high-grade gliomas: complications and pitfalls, J Neurooncol 107(2) (2012) 373-8.

[53] M.L. Brady, R. Raghavan, W. Block, B. Grabow, C. Ross, K. Kubota, A.L. Alexander, M.E. Emborg, The Relation between Catheter Occlusion and Backflow during Intraparenchymal Cerebral Infusions, Stereotact Funct Neurosurg 93(2) (2015) 102-109.

[54] W.Y. Su, Y.C. Chen, F.H. Lin, Injectable oxidized hyaluronic acid/adipic acid dihydrazide hydrogel for nucleus pulposus regeneration, Acta Biomater 6(8) (2010) 3044-55.

[55] E.J. Cho, B. Sun, K.O. Doh, E.M. Wilson, S. Torregrosa-Allen, B.D. Elzey, Y. Yeo, Intraperitoneal delivery of platinum with in-situ crosslinkable hyaluronic acid gel for local therapy of ovarian cancer, Biomaterials 37 (2015) 312-9.

[56] X. Wang, J. Wang, W. Wu, H. Li, Vaginal delivery of carboplatin-loaded thermosensitive hydrogel to prevent local cervical cancer recurrence in mice, Drug Deliv 23(9) (2016) 3544-3551.

doi:10.6342/NTU201704398

[57] J.Y. Fang, J.P. Chen, Y.L. Leu, J.W. Hu, The delivery of platinum drugs from thermosensitive hydrogels containing different ratios of chitosan, Drug Deliv 15(4) (2008) 235-43.

[58] J.P. Chen, Y.L. Leu, C.L. Fang, C.H. Chen, J.Y. Fang, Thermosensitive hydrogels composed of hyaluronic acid and gelatin as carriers for the intravesical administration of cisplatin, J Pharm Sci 100(2) (2011) 655-66.

[59] H.T. Liang, X.S. Lai, M.F. Wei, S.H. Lu, W.F. Wen, S.H. Kuo, C.M. Chen, W.I. Tseng, F.H. Lin, Intratumoral injection of thermogelling and sustained-release carboplatin-loaded hydrogel simplifies the administration and remains the synergistic effect with radiotherapy for mice gliomas, Biomaterials 151 (2018) 38-52.

[60] M.D. Walker, E. Alexander Jr, W.E. Hunt, C.S. MacCarty, M.S. Mahaley Jr, J. Mealey Jr, H.A. Norrell, G. Owens, J. Ransohoff, C.B. Wilson, Evaluation of BCNU and/or radiotherapy in the treatment of anaplastic gliomas: a cooperative clinical trial, Journal of neurosurgery 49(3) (1978) 333-343.

[61] K.L. Chaichana, J.C. Martinez-Gutierrez, R. De la Garza-Ramos, J.D. Weingart, A. Olivi, G.L. Gallia, M. Lim, H. Brem, A. Quinones-Hinojosa, Factors associated with survival for patients with glioblastoma with poor pre-operative functional status, J Clin Neurosci 20(6) (2013) 818-23.

[62] P. Linhares, B. Carvalho, R. Figueiredo, R.M. Reis, R. Vaz, Early Pseudoprogression following Chemoradiotherapy in Glioblastoma Patients: The Value of RANO Evaluation, J Oncol 2013 (2013) 690585.

[63] P.Y. Wen, D.R. Macdonald, D.A. Reardon, T.F. Cloughesy, A.G. Sorensen, E. Galanis, J. DeGroot, W. Wick, M.R. Gilbert, A.B. Lassman, Updated response assessment criteria for

doi:10.6342/NTU201704398

high-grade gliomas: response assessment in neuro-oncology working group, Journal of Clinical Oncology 28(11) (2010) 1963-1972.

[64] H.T. Liang, W.Y. Chen, S.F. Lai, M.Y. Su, S.L. You, L.H. Chen, H.M. Tseng, C.M. Chen, S.H. Kuo, W.I. Tseng, The extent of edema and tumor synchronous invasion into the subventricular zone and corpus callosum classify outcomes and radiotherapy strategies of glioblastomas, Radiother Oncol (2017).

[65] S. Raysi Dehcordi, D. De Paulis, S. Marzi, A. Ricci, A. Cimini, M.G. Cifone, R.J. Galzio, Survival prognostic factors in patients with glioblastoma: our experience, J Neurosurg Sci 56(3) (2012) 239-45.

[66] G. Bajaj, M.R. Kim, S.I. Mohammed, Y. Yeo, Hyaluronic acid-based hydrogel for regional delivery of paclitaxel to intraperitoneal tumors, J Control Release 158(3) (2012) 386-92.

[67] W.Y. Su, K.H. Chen, Y.C. Chen, Y.H. Lee, C.L. Tseng, F.H. Lin, An injectable oxidated hyaluronic acid/adipic acid dihydrazide hydrogel as a vitreous substitute, J Biomater Sci Polym Ed 22(13) (2011) 1777-97.

[68] W. Shen, J. Luan, L. Cao, J. Sun, L. Yu, J. Ding, Thermogelling polymer-platinum(IV) conjugates for long-term delivery of cisplatin, Biomacromolecules 16(1) (2015) 105-15.

[69] Biological evaluation of medical devices. Part 5. Test for cytotoxicity: in vitro methods., in: I.S. Organization (Ed.) ISO 10993-5, 2009.

[70] T. Fourniols, L.D. Randolph, A. Staub, K. Vanvarenberg, J.G. Leprince, V. Preat, A. des Rieux, F. Danhier, Temozolomide-loaded photopolymerizable PEG-DMA-based hydrogel for the treatment of glioblastoma, J Control Release 210 (2015) 95-104.

doi:10.6342/NTU201704398

[71] C. Bastiancich, K. Vanvarenberg, B. Ucakar, M. Pitorre, G. Bastiat, F. Lagarce, V. Preat, F. Danhier, Lauroyl-gemcitabine-loaded lipid nanocapsule hydrogel for the treatment of glioblastoma, J Control Release 225 (2016) 283-93.

[72] T. Arai, O. Benny, T. Joki, L.G. Menon, M. Machluf, T. Abe, R.S. Carroll, P.M. Black, Novel local drug delivery system using thermoreversible gel in combination with polymeric microspheres or liposomes, Anticancer research 30(4) (2010) 1057-1064.

[73] S.C. Wang, J.H. Hong, C. Hsueh, C.S. Chiang, Tumor-secreted SDF-1 promotes glioma invasiveness and TAM tropism toward hypoxia in a murine astrocytoma model, Lab Invest 92(1) (2012) 151-62.

[74] P.S. Jiang, C.F. Yu, C.Y. Yen, C.W. Woo, S.H. Lo, Y.K. Huang, J.H. Hong, C.S. Chiang, Irradiation Enhances the Ability of Monocytes as Nanoparticle Carrier for Cancer Therapy, PLoS One 10(9) (2015) e0139043.

[75] E.S. Lee, H.J. Im, H.S. Kim, H. Youn, H.J. Lee, S.U. Kim, D.W. Hwang, D.S. Lee, In vivo brain delivery of v-myc overproduced human neural stem cells via the intranasal pathway: tumor characteristics in the lung of a nude mouse, Mol Imaging 13 (2014).

[76] W.L. Wang, S.Y. Sheu, Y.S. Chen, S.T. Kao, Y.T. Fu, T.F. Kuo, K.Y. Chen, C.H. Yao, Enhanced Bone Tissue Regeneration by Porous Gelatin Composites Loaded with the Chinese Herbal Decoction Danggui Buxue Tang, PLoS One 10(6) (2015) e0131999.

[77] C.H. Chou, C.M. Teng, K.Y. Tzen, Y.C. Chang, J.H. Chen, J.C. Cheng, MMP-9 from sublethally irradiated tumor promotes Lewis lung carcinoma cell invasiveness and pulmonary metastasis, Oncogene 31(4) (2012) 458-68.

doi:10.6342/NTU201704398

[78] T.M. Krupka, B.D. Weinberg, H. Wu, N.P. Ziats, A.A. Exner, Effect of intratumoral injection of carboplatin combined with pluronic P85 or L61 on experimental colorectal carcinoma in rats, Exp Biol Med (Maywood) 232(7) (2007) 950-7.

[79] M.M. Tomayko, C.P. Reynolds, Determination of subcutaneous tumor size in athymic (nude) mice, Cancer chemotherapy and pharmacology 24(3) (1989) 148-154.

[80] Y. Inoue, S. Kiryu, M. Watanabe, A. Tojo, K. Ohtomo, Timing of imaging after d-luciferin injection affects the longitudinal assessment of tumor growth using in vivo bioluminescence imaging, Int J Biomed Imaging 2010 (2010) 471408.

[81] K. Suchowski, T. Poschinger, A. Rehemtulla, M. Sturzl, W. Scheuer, Noninvasive Bioluminescence Imaging of AKT Kinase Activity in Subcutaneous and Orthotopic NSCLC Xenografts: Correlation of AKT Activity with Tumor Growth Kinetics, Neoplasia 19(4) (2017) 310-320.

[82] Z.H. Siddik, M. Jones, F.E. Boxall, K.R. Harrap, Comparative distribution and excretion of carboplatin and cisplatin in mice, Cancer Chemother Pharmacol 21(1) (1988) 19-24.

[83] R. Wysokiński, J. Kuduk-Jaworska, D. Michalska, Electronic structure, Raman and infrared spectra, and vibrational assignment of carboplatin. Density functional theory studies, Journal of Molecular Structure: THEOCHEM 758(2) (2006) 169-179.

[84] S.H. Poulsen, T. Urup, K. Grunnet, I.J. Christensen, V.A. Larsen, M.L. Jensen, P.M. Af Rosenschold, H.S. Poulsen, I. Law, The prognostic value of FET PET at radiotherapy planning in newly diagnosed glioblastoma, Eur J Nucl Med Mol Imaging (2016).

[85] M. Harat, B. Malkowski, R. Makarewicz, Pre-irradiation tumour volumes defined by MRI and dual time-point FET-PET for the prediction of glioblastoma multiforme recurrence: A prospective study, Radiother Oncol 120(2) (2016) 241-7.

doi:10.6342/NTU201704398

[86] K. Reddy, L.E. Gaspar, B.D. Kavanagh, C. Chen, Hypofractionated intensity-modulated radiotherapy with temozolomide chemotherapy may alter the patterns of failure in patients with glioblastoma multiforme, J Med Imaging Radiat Oncol 58(6) (2014) 714-21.

[87] T. Iuchi, K. Hatano, T. Kodama, T. Sakaida, S. Yokoi, K. Kawasaki, Y. Hasegawa, R. Hara, Phase 2 trial of hypofractionated high-dose intensity modulated radiation therapy with concurrent and adjuvant temozolomide for newly diagnosed glioblastoma, Int J Radiat Oncol Biol Phys 88(4) (2014) 793-800.

[88] M. Farzin, M. Molls, S. Astner, I.C. Rondak, M. Oechsner, Simultaneous integrated vs. sequential boost in VMAT radiotherapy of high-grade gliomas, Strahlenther Onkol 191(12) (2015) 945-52.

[89] G. Truc, V. Bernier, C. Mirjolet, C. Dalban, F. Mazoyer, F. Bonnetain, N. Blanchard, E. Lagneau, P. Maingon, G. Noel, A phase I dose escalation study using simultaneous integrated-boost IMRT with temozolomide in patients with unifocal glioblastoma, Cancer Radiother 20(3) (2016) 193-8.

[90] L. Chen, H. Guerrero-Cazares, X. Ye, E. Ford, T. McNutt, L. Kleinberg, M. Lim, K. Chaichana, A. Quinones-Hinojosa, K. Redmond, Increased subventricular zone radiation dose correlates with survival in glioblastoma patients after gross total resection, International journal of radiation oncology, biology, physics 86(4) (2013) 616-22.

[91] P. Evers, P.P. Lee, J. DeMarco, N. Agazaryan, J.W. Sayre, M. Selch, F. Pajonk, Irradiation of the potential cancer stem cell niches in the adult brain improves progression-free survival of patients with malignant glioma, BMC cancer 10 (2010) 384.

doi:10.6342/NTU201704398

[92] J. Unkelbach, B.H. Menze, E. Konukoglu, F. Dittmann, M. Le, N. Ayache, H.A. Shih, Radiotherapy planning for glioblastoma based on a tumor growth model: improving target volume delineation, Physics in medicine and biology 59(3) (2014) 747-70.

[93] M. Mizumoto, T. Yamamoto, E. Ishikawa, M. Matsuda, S. Takano, H. Ishikawa, T. Okumura, H. Sakurai, A. Matsumura, K. Tsuboi, Proton beam therapy with concurrent chemotherapy for glioblastoma multiforme: comparison of nimustine hydrochloride and temozolomide, J Neurooncol 130(1) (2016) 165-170.

[94] M.M. Hsiang-Kuang Tony Liang, Tetsuya Yamamoto, Daich Takizawa, Keiich Tanaka, Teruhito Aihara, Toshiyuki Okumura, Hitoshi Ishikawa, Koji Tsuboi, Hideyuki Sakurai, Edema extent of glioblastoma determined the survival and progression pattern after high-dose proton beam boost, Particle Therapy Co-Operative Group, Yokohama, Japan, 2017.

[95] X.F. Wang, G.S. Lin, Z.X. Lin, Y.P. Chen, Y. Chen, J.D. Zhang, W.L. Tan, Association of pSTAT3-VEGF signaling pathway with peritumoral edema in newly diagnosed glioblastoma: an immunohistochemical study, Int J Clin Exp Pathol 7(9) (2014) 6133-40.

[96] S. Takano, H. Kimu, K. Tsuda, S. Osuka, K. Nakai, T. Yamamoto, E. Ishikawa, H. Akutsu, M. Matsuda, A. Matsumura, Decrease in the apparent diffusion coefficient in peritumoral edema for the assessment of recurrent glioblastoma treated by bevacizumab, Acta Neurochir Suppl 118 (2013) 185-9.

[97] D.V. Brown, P.M. Daniel, G.M. D'Abaco, A. Gogos, W. Ng, A.P. Morokoff, T. Mantamadiotis, Coexpression analysis of CD133 and CD44 identifies proneural and mesenchymal subtypes of glioblastoma multiforme, Oncotarget 6(8) (2015) 6267-80.

[98] S.G. Piccirillo, I. Spiteri, A. Sottoriva, A. Touloumis, S. Ber, S.J. Price, R. Heywood, N.J. Francis, K.D. Howarth, V.P. Collins, A.R. Venkitaraman, C. Curtis, J.C. Marioni, S.

doi:10.6342/NTU201704398

Tavare, C. Watts, Contributions to drug resistance in glioblastoma derived from malignant cells in the sub-ependymal zone, Cancer research 75(1) (2015) 194-202.

[99] K. Wang, Y. Wang, X. Fan, J. Wang, G. Li, J. Ma, J. Ma, T. Jiang, J. Dai, Radiological features combined with IDH1 status for predicting the survival outcome of glioblastoma patients, Neuro Oncol 18(4) (2016) 589-97.

[100] J. Carrillo, A. Lai, P. Nghiemphu, H. Kim, H. Phillips, S. Kharbanda, P. Moftakhar, S. Lalaezari, W. Yong, B. Ellingson, Relationship between tumor enhancement, edema, IDH1 mutational status, MGMT promoter methylation, and survival in glioblastoma, American Journal of Neuroradiology 33(7) (2012) 1349-1355.

[101] A. Kakita, M. Zerlin, H. Takahashi, J.E. Goldman, Some glial progenitors in the neonatal subventricular zone migrate through the corpus callosum to the contralateral cerebral hemisphere, J Comp Neurol 458(4) (2003) 381-8.

[102] A. Kakita, M. Zerlin, H. Takahashi, J.E. Goldman, Some glial progenitors in the neonatal subventricular zone migrate through the corpus callosum to the contralateral cerebral hemisphere, Journal of Comparative Neurology 458(4) (2003) 381-388.

doi:10.6342/NTU201704398

APPENDIX

A. Abbreviations

3DCRT, three-dimensional conformal radiotherapy

AC, aqueous carboplatin

ACR, radiotherapy with aqueous carboplatin

ADH, adipic acid dihydrazide

ANOVA, analysis of variance

BCNU, bis-chloroethylnitrosourea

BCS, blood biochemistry study

BLI, bioluminescence imaging

BTV, biological tumor volume

CBC, complete blood count

CC, corpus callosum

CCEPD, extensive progressive disease along the corpus callosum

CCEPE, extensive preoperative edema along the corpus callosum

CCRT, concurrent chemoradiotherapy

CED, convection-enhanced delivery

CI, confidence interval

CT, computed tomography

CTV, clinical target volume

DNA, deoxyribonucleic acid

EthD-1, ethidium homodimer

EORTC, European Organisation for Research and Treatment of Cancer

doi:10.6342/NTU201704398

EPD, extensive progressive disease

EPE, extensive preoperative edema

FLAIR, fluid-attenuated inversion recovery

FTIR, Fourier transformation infrared

KPS, Karnofsky performance status

Gr, group

GTV, gross tumor volume

H, hydrogel

H&E, hematoxylin and eosin

HC, hydrogel carboplatin

HCR, radiotherapy with hydrogel carboplatin

HR, hazard ratio

HRT, radiotherapy with hydrogel

IC_{50}, half maximal inhibitory concentration

ICP-MS, inductively coupled plasma mass spectrometry

IDH1, isocitrate dehydrogenase 1

IMRT, intensity-modulated radiation therapy

IVIS, In Vivo Image System

LDH, lactate dehydrogenase

LPD, local progressive disease

MGMT, O^6-methylguanin-DNA methyltransferase

MOS, median overall survival

MPFS, median progression-free survival

doi:10.6342/NTU201704398

MRI, magnetic resonance imaging

N, number

NFT, neural fiber tract

OS, overall survival

Oxi-HA, oxidized hyaluronic acid

Oxi-HA/ADH, oxidated hyaluronic acid/adipic acid dihydrazide

R/RT, radiotherapy

PD, progressive disease

PE, preoperative edema

PFS, progression-free survival

Pre-OP, preoperative

RTOG, Radiation Therapy Oncology Group

S, shame

SIB, simultaneous integrated boost

SVZ, subventricular zone

sSVZCC, synchronous subventricular zone and corpus callosum

SVZEPD, extensive progressive disease along the subventricular zone

SVZEPE, extensive preoperative edema along the subventricular zone

T1W+C, contrast-enhanced T1-weighted magnetic resonance imaging

TM, tumor margin

TMZ, temozolomide

VMAT, volumetric-modulated arc therapy

WST-1, water soluble tetrazolium-1

doi:10.6342/NTU201704398

B. Publications

B1. Original Articles

1. **Hsiang-Kuang Tony Liang**, Xue-Shi Lai, Ming-Feng Weib, Szu-Huai Lu, Wen-Fen Wen, Sung-Hsin Kuo, Chung-Ming Chen, Wen-Yih Isaac Tseng, and Feng-Huei Lin. Intratumoral injection of thermogelling and sustained-release carboplatin-loaded hydrogel simplifies the administration and remains the synergistic effect with radiotherapy for mice gliomas. *Biomaterials*, doi: 10.1016/j.biomaterials.2017.10.015
2. **Hsiang-Kuang Tony Liang**, Wan-Yu Chen, Shih-Fan Lai, Mao-Yuan Su, San-Lin You, Liang-Hsin Chen, Ham-Min Tseng, Chung-Ming Chen, Sung-Hsin Kuo, and Wen-Yih Isaac Tseng. The extent of edema and tumor synchronous invasion into the subventricular zone and corpus callosum classify outcomes and radiotherapy strategies of glioblastomas. *Radiotherapy and Oncology*, doi: 10.1016/j.radonc.2017.09.024
3. **Tony Hsiang-Kuang Liang**, Sung-Hsin Kuo, Chun-Wei Wang, Wan-Yu Chen, Che-Yu Hsu, Shih-Fan Lai, Ham-Min Tseng, San-Lin You, Chung-Ming Chen, and Wen-Yih Isaac Tseng. Adverse prognosis and distinct progression patterns after concurrent chemoradiotherapy for glioblastoma with synchronous subventricular zone and corpus callosum invasion. *Radiotherapy and Oncology.* 2016; 118:16–23.
4. Chen WY, Kuo SH, Shen CW, Huang BS, Lan KH, **Liang HK**, Wang CW. Good tolerance and long-term complete remission after definitive intensity-modulated radiotherapy for locally advanced head and neck cancer in a patient with human immunodeficiency virus infection: A case report and literature review. *Head Neck.* 2015.2015;37(12):E186-90.
5. Wang CW, Lin YC, Tseng HM, Xiao F, Chen CM, Cheng WL, Lu SH, Lan KH, Chen

doi:10.6342/NTU201704398

WY, **Liang HK**, Kuo SH. Prolonged treatment time deteriorates positioning accuracy for stereotactic radiosurgery. *PLoS One*. 2015;10(4): e0123359. doi: 10.1371.

6. **Liang HK**, Wang CW, Tseng HM, Huang CY, Lan KH, Chen YH, You SL, Cheng JC, Cheng AL, Kuo SH. Preoperative Prognostic Neurologic Index for Glioblastoma Patients Receiving Tumor Resection. *Ann Surg Oncol*. 2014; 21:3992-3998.
7. **Hsiang-Kuang Liang**, Chao-Yuan Huang, Chun-Wei Wang, Yu-Hsuan Chen, Sung-Hsin Kuo, Jason Chia-Hsien. Cheng Clinical Characteristics, Image Findings, and Treatment Modalities Associate with Outcomes of Patients with Glioblastoma Multiforme. *Therapeutic Radiology and Oncology*; 2012; 19:93-104

B2. Oral Presentations

1. American Society for Radiation Oncology 59th Annual Meeting, 2017: **Hsiang-Kuang Tony Liang**, Wan-Yu Chen, Shih-Fan Lai, Mao-Yuan Su, San-Lin You, Liang-Hsin Chen, Ham-Min Tseng, Chung-Ming Chen, Sung-Hsin Kuo, Wen-Yih Isaac Tseng The extent of edema and tumor synchronous invasion into the subventricular zone and corpus callosum classify outcomes and radiotherapy strategies of glioblastomas (accepted, ePoster with oral presentation)
2. 5th Japan Taiwan Radiation Oncology Symposium, 2017: **Hsiang-Kuang Tony Liang**, Sung-Hsin Kuo, Chun-Wei Wang, Wan-Yu Chen, Che-Yu Hsu, Shih-Fan Lai, b, Ham-Min Tseng, San-Lin You, Chung-Ming Chen, and Wen-Yih Isaac Tseng. Adverse Prognosis and Distinct Progression Patterns After Concurrent Chemoradiotherapy for Glioblastoma With Synchronous Subventricular Zone and Corpus Callosum Invasion, Updated Report

doi:10.6342/NTU201704398

3. 56th Annual Conference of Particle Therapy Co-operative Group, Oral Presentation, 2017: **Hsiang-Kuang Tony Liang**, Masashi Mizumoto, Tetsuya Yamamoto, Daich Takizawa, Keiich Tanaka, Teruhito Aihara, Toshiyuki Okumura, Hitoshi Ishikawa, Koji Tsuboi, Hideyuki Sakurai. Edema extent of glioblastoma determined the survival and progression pattern after concurrent chemoradiotherapy with proton beam.

B3. Posters

1. Taiwan Neurology Society Annual Meeting, 2010: **Hsiang-Kuang Liang**, Chun-Wei Wang, Jason Chia-Hsien. Case presentation: The use of intensity-modulated radiation therapy for a 26-year-old woman with recurrent nasopharyngeal angiofibroma.
2. Taiwan Neurology Society Annual Meeting, 2009: **Hsiang-Kuang Liang**, Chao-Yuan Huang. Case presentation: The use of helical tomotherapy for a 43-year-old man with medulloblastoma. (The first case treated by helical tomotherapy in National Taiwan University Hospital)
3. Taiwan Neurology Society Annual Meeting, 2008: **Hsiang-Kuang Liang**, Ming-Jang Chiu. Case presentation: A 67-year-old man who was found to have undetermined metastatic tumors with the initial presentation of embolic cerebral infarct.
4. Taiwan Neurology Society Annual Meeting, 2007: **Hsiang-Kuang Liang**, Chi-Chao Chao, Sung-Tsang Hsieh. Systemic lupus erythematosus initially presented as myasthenia gravis, mononeuropathy multiplex, cerebral infarct and cutaneous vasculitis - a case report.
5. Taiwan Neurology Society Annual Meeting, 2006: **Hsiang-Kuang Liang**, Ming-Jang Chiu. Myotonia congenita-a case report.

doi:10.6342/NTU201704398